POLITECNICO DI TORINO

Master’s degree

in Nanotechnologies for ICTs

Master’s Degree Thesis

Modelling of Spin Torque Nano-Oscillators with perpendicular polarizer and planar free layer

Supervisors
Ursula Ebels
Liliana Prejbeanu

Candidate
Mateo David Ibarra Gómez

PoliTO Responsible
prof. Carlo Ricciardi

October 13, 2020

Table of contents

1. Introduction

The spin of electrons and its interaction with the local magnetization of a ferromagnetic material is of great interest for current and future research, because it has offered and continues to offer a large variety of applications. Spin Torque Nano-Oscillators (STNO) are a result of this research and they promise improvements in different areas of technology like wireless communications and machine learning. The basics of the physics of a single one of these oscillators is relatively well understood, but it is still necessary to comprehend in a fundamental manner how the synchronization of a coupled network of these devices works. This is a complex task because of different reasons: first, a large range of parameters come into play. The synchronization depends on the geometry of the network and that of each device. It is also influenced by the type of coupling being used that can be via the RF current or an RF field, and there are external control parameters like the injected DC current and the applied magnetic field that affect the excitation mode (amplitude, frequency..) and through this the coupling. Secondly, different dynamical states can result from the interaction between oscillators among which: fully coherent, chimera and chaotic. Thirdly, since a network implies several devices interacting with one another, it is necessary to introduce and apply concepts from non-linear dynamical systems to advance in this understanding. This study is important because, when considered as a network, these oscillators are expected to improve their output power and to diminish their phase noise which are important parameters for communications applications. Moreover, the different dynamical states of the network have the potential for being used in machine learning.

In this context, the aim of this master's thesis project was to study the dynamics of a single STNO, then the coupling to an external signal through injection locking, and the synchronization through dipolar interaction of two spin torque nano-oscillators. Additionally, a specific STNO structure was selected, based on a Magnetic Tunnel Junction and composed of a perpendicular magnetized polarizer, an in-plane magnetized free layer and a perpendicular applied field (these will be explained later). This structure is of interest because it leads to symmetric trajectories of the magnetization, which allows for mathematical simplicity; in the second place, it gives rise to larger amplitudes of oscillation that allow for better dipolar coupling for synchronization. The numerical study of this STNO system was undertaken using the Landau-Lifshitz-Gilbert-Slonczewski (LLGS) equation that governs the dynamics of the magnetization under spin-transfer-torque. Several parameters were varied in order to understand their effect on the dynamics such as the geometry of the device, the current density and external magnetic field, and the separation between oscillators. The numerical simulation code employed for this purpose was provided by SPINTEC and the project is envisioned to continue with a PhD.

SPINTEC is a spintronics research lab operated by CEA, CNRS and the University of Grenoble Alpes. It aims towards the technology and science research applied to spintronics. This master thesis was done with one of SPINTEC's groups that is oriented towards RF concepts.

2. Basic concepts

2.1 Spin polarized current

Spintronics is the field of nanoelectronics that exploits the spin degree of freedom of electrons and its interaction with the local magnetization enabling either the control of the flow of electrons and/or the control of the magnetization of a system. Different interesting spintronics phenomena can be distinguished. Underlying most of them is the existence of a **spin polarized current** where there is a nonzero spin polarization average of the flowing electrons per unit time. This takes place in ferromagnetic materials, where there is a shift between spin-up and the spin-down electron bands as shown in figure 1. Thus, there is a majority population of (localized) electrons (spin-up) and a minority one (spin-down) making up the total magnetic moment **M**. Moreover, when a current is injected, spin-down conduction (delocalized) electrons scatter more because there are more empty states to scatter into in the density of states of electrons with this spin polarization, as can be noted in figure 1. Hence, a current with a finite spin polarization arises. To illustrate this: when an unpolarized current is injected into a ferromagnetic material, it becomes spin polarized after a certain average length, called the spin diffusion length, which is on the order of a few nanometers. [1]

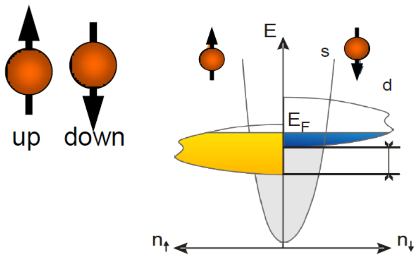

Fig. 1: Schematics of the density of states of spin-up and spin-down electrons.

2.2 Magneto-resistance

The existence of a spin polarized current results in several important phenomena. The first is the **magnetoresistance** (MR), which is the change in the resistance of a structure due to the variation in the relative magnetization orientations of different magnetic layers within a magnetoresistive device.

One basic structure is a **magnetic tunnel junction** (MTJ), left of figures 2a and 2b; this MTJ is composed of two ferromagnetic layers called hereafter *electrodes*. One layer is referred to as the *polarizer* (Pol) and the other is the *free layer* (FL); the thickness of them is of a few nanometers. These two ferromagnetic layers are separated by a spacer layer of an insulating material, generally MgO, called the *tunnel barrier*. The MgO spacer is quite thin (1nm). Since it is an insulator, it introduces an energy barrier between the electrodes which favors quantum tunneling and hence, this is the phenomenon that dominates the transport of electrons (i.e. the resistance) between these two ferromagnetic layers. This raises another question: what happens with the spin of the electrons after tunneling? According to a model proposed by Julliere [2], after tunneling, the electrons conserve their spin polarization, so that if it was spin up before tunneling, it will keep the same spin afterwards. This will be used for analyzing two different cases of the direction of magnetization of the electrodes: a parallel or antiparallel configuration, figure 2. For the first case, the orientation of the majority electrons, is the same in both layers, as can be seen in figure 2a, thus, when a voltage is applied, due to the greater amount of occupied and empty states in the polarizer and the free layer respectively, the resistance, will be smaller and thus the spin polarized current will be larger. For the second case, since electrons with the same spin are majority in one layer and minority in the other, as shown in figure 2b, there are less states available for tunneling with respect to the previous situation and therefore the resistance, R will be larger and the spin polarized current smaller. This situation where the tunneling current is affected by the magnetization state takes the name of **tunneling magnetoresistance** (TMR), quantified by the ratio from relation (1), where R_{AP} is the resistance in the antiparallel configuration and R_P the resistance in the parallel one.

$$TMR = \frac{R_{AP} - R_p}{R_p} \qquad (1)$$

(a) Parallel configuration

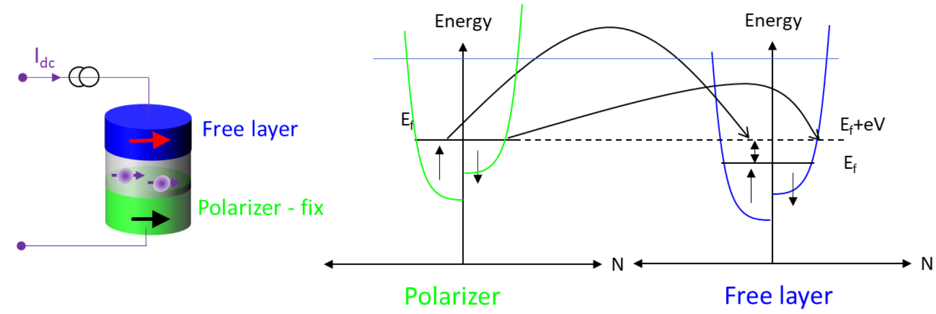

(b) Antiparallel configuration

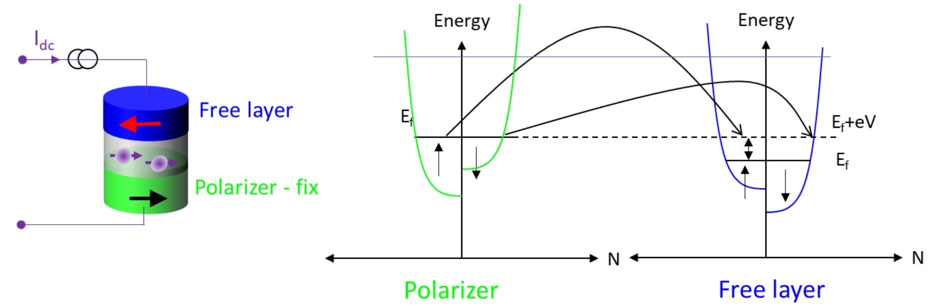

Fig. 2: Tunneling Magnetoresistance. Between the Polarizer and the Free Layer an energy barrier potential has been introduced through an applied voltage.

2.3 Spin momentum transfer

So far, we have seen how the magnetization of a device acts on the spin polarized current giving rise to the magnet-resistance (MR). **Spin transfer torque** (STT) is the name given to the reciprocal phenomenon: the spin polarized current affects the magnetization. This happens because the spin polarized electrons transmitted to the free layer from the polarizer transfer spin angular momentum to the local magnetization changing its direction; thus, this transfer of momentum is equivalent to a pseudo-torque acting on the magnetization which has to be taken into account in the equation of motion of the magnetization, as discussed in the next section.

It is worth mentioning here first that in the preceding paragraphs we have been talking about the magnetization of the ferromagnetic layers as being represented by just one magnetization direction. This is not the real case, but a simplified model called **macrospin approximation,** in which one considers a sample of dimensions small enough so that there is no multi-domain structure but a single domain, represented by one magnetization vector, i.e. each layer in the MTJ structure is represented by one magnetization vector. We will use this macrospin approach throughout the thesis.

2.4 Magnetization dynamics

The coordinate system that will be used with respect to the MTJ is shown in figure 3a. Furthermore the magnetization is represented by a vector **M** that is the average of the magnetic moment μ_i over an elementary volume dV: $\boldsymbol{M} = \sum_i \frac{\mu_i}{dV}$. **M** can also be expressed as $M_s\mathbf{m}$, where M_s is the spontaneous magnetization, that is constant for a given temperature, and **m** is the unitary vector related to the direction of the magnetization **m** = (m_x, m_y, m_z). Therefore, only **m** changes and it evolves on a unit sphere, figure 3b. Moreover, in the real case **m** is a function of the position ***r*** in the material and time *t,* but within the macrospin approximation and within the same magnetic layer, it is only function of *t*.

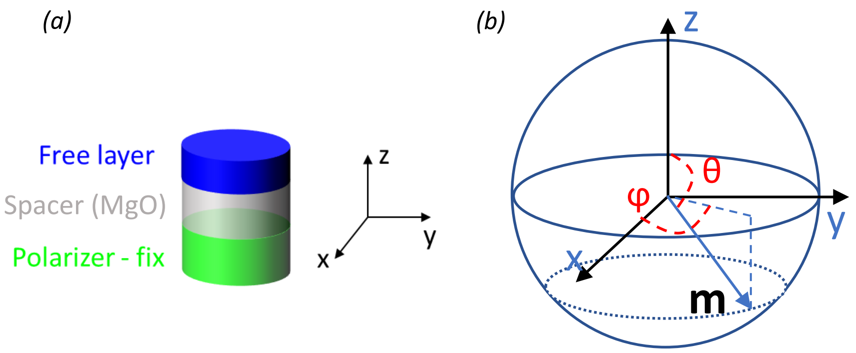

Fig 3. (a) depicts the MTJ structure and the coordinate system used throughout this thesis. In (b) the unit sphere of **m** is sketched.

2.4.1 Gibbs free energy

For the understanding of the magnetization dynamics it is fundamental to get an idea about the different contributions to the magnetic energy as detailed below [3].

(i) The Zeeman energy, E_z, which is due to the external applied field $\mathbf{H_{app}}$.

(ii) The dipolar or demagnetising energy, E_d, coming from the fact that each magnetic moment produces a stray field that tries to align the other magnetic moments parallel to this stray field. This entails a long-range interaction.

(iii) The magnetocrystalline anisotropy (MCA) energy, E_{anis}, for which the magnetization minimizes its energy when oriented along certain symmetry directions (the easy axes). For the simplest case, the uniaxial anisotropy, there is only one easy axis. This is the most common situation and the one considered in this thesis.

(iv) The exchange energy, that comes from the exchange interaction, a quantum mechanical effect which is important in short-range distances and couples neighbouring spins to be parallel in ferromagnets. The competition of this interaction with the dipolar one accounts for the domain structure and their relative strengths determine the size of magnetic domains and the domain walls.

(v) The energy due to the Oersted field, produced from the flow of a current through a nanostructure device.

(vi) The energy related to the magnetoelastic interaction that accounts for the effect that magnetic fields and the mechanical stress have on each other, but this is negligible for the materials considered in this thesis.

(vii) The thermal energy, due to stochastic thermal fluctuations.

It is important to mention that in this thesis, because of the macrospin approximation (with spins aligned all parallel to each other), the exchange energy, which is important when adjacent magnetic moments are not parallel, is discarded. Moreover, since the Oersted field is not uniform, i.e., it points in different directions depending on the position with respect to the current, it will not be considered either. The magneto-elastic contribution is also neglected.

The effect of the demagnetizing energy is taken into account through a 3x3-demagnetization tensor whose components depend on the geometrical shape of the magnetic body. A thin magnetic film may be modelled as a uniformly magnetised ellipsoid of revolution, which is a single domain structure [4-6] whose demagnetization tensor is diagonal if expressed in the basis of the principal axes, eq. 2. Moreover, the value of N_{xx}, N_{yy} or N_{zz}, is lower when the dimension along x, y or z is larger respectively, i.e. $N_{xx} < N_{yy} < N_{zz}$, for lengths $L_x > L_y > L_z$. This implies that the dipolar energy is minimized along the largest dimensions. This is called *shape anisotropy*.

$$N = \begin{pmatrix} N_{xx} & 0 & 0 \\ 0 & N_{yy} & 0 \\ 0 & 0 & N_{zz} \end{pmatrix} \text{ with } N_{xx} + N_{yy} + N_{zz} = 1 \quad (2)$$

The energy density expression which is considered in this thesis is given in eq. 3c. 3c has its terms in the same order as 3a, $\boldsymbol{u_K}$ is the direction of the easy axis, K_u is the anisotropy energy constant and μ_0 is the permeability of free space. Besides, the total energy in the macrospin approximation is given by eq. 3c where *V* is the volume.

$$E = E_z + E_d + E_{anis} \qquad (3a)$$

$$E = E_{density} V \qquad (3b)$$

$$E_{density} = -\mu_0 M_s \boldsymbol{m} \cdot \boldsymbol{H_{app}} + \frac{1}{2}\mu_0 M_s^2 \left(N_{xx} m_x^2 + N_{yy} m_y^2 + N_{zz} m_z^2\right) + K_u [1 - (\boldsymbol{u_K} \cdot \boldsymbol{m})^2] \quad (3b)$$

Figures 4a and 4b show the energy density of a thin magnetic film respectively without and with magnetocrystalline anisotropy along the *x* direction. Spherical coordinates were used, and as in the rest of this thesis θ is the polar angle from the z axis and φ is the azimuthal angle from the x-axis along the xy plane which is in-plane (see Fig. 4). The energy minima, for the two figures, are at θ = π /2, the in-plane orientation, because this is the direction of the largest dimension, which as mentioned before, minimizes the demagnetisation energy. In figure 4a, since there is no anisotropy, the energy minimum in θ = π /2 does not have a preferred value of φ, i.e. it is isotropic in the in-plane direction. In the situation of figure 4b the presence of an easy axis in the x direction produces two energy minima for θ = π /2: one in φ = 0 and the other in φ = π. In both figures the energy maxima are when the magnetization is oriented in the positive or negative z directions, which corresponds to θ = 0 and θ = π.

2.4.2 Effective field

Another important concept is the effective field, defined by the equation 4a; It is proportional to the variational derivative of the energy density with respect to the magnetization. Due to its relation with the energy (3a), its contributions come from the same phenomena as shown in equation 4b.

$$\boldsymbol{H_{eff}} = -\frac{1}{\mu_0}\frac{\delta E_{density}}{\delta \boldsymbol{M}} \quad (4a)$$

$$\boldsymbol{H_{eff}} = \boldsymbol{H_{app}} + \boldsymbol{H_d} + \boldsymbol{H_{anis}} \quad (4b)$$

Figures 4a and 4b show the energy density in absence of an applied field. But it is also important to see how an applied magnetic field changes this energy landscape; with this purpose figures 4c and 4d show the energy density map for the case of zero anisotropy (such as figure 4a) with a magnetic field applied in plane (Fig. 4c) and out of plane (Fig. 4d) respectively. In the first case, since the field is oriented in the φ = 0 direction, the two energy minima at φ = 0 and φ =180 are no more degenerate, the one at φ = 0 becomes the global and the one at φ = 180 becomes a local minimum. In the second case, the energy along φ does not change as was the case in figure 4a, but there are two differences: the required energy for taking the magnetization out of plane, that is, θ = 0, is decreased with respect to 4a; in the second place, thanks to the out of plane magnetic field, the energy minimum is not anymore along θ = π /2, but it is slightly shifted towards the positive z direction. Furthermore, one can note that for all these considered cases, the minima of the energy were determined by the direction of the effective field that comprises the contributions from the anisotropy, the demagnetising field and the external magnetic field. Thus, the magnetisation had to be aligned with this effective field to minimize its energy.

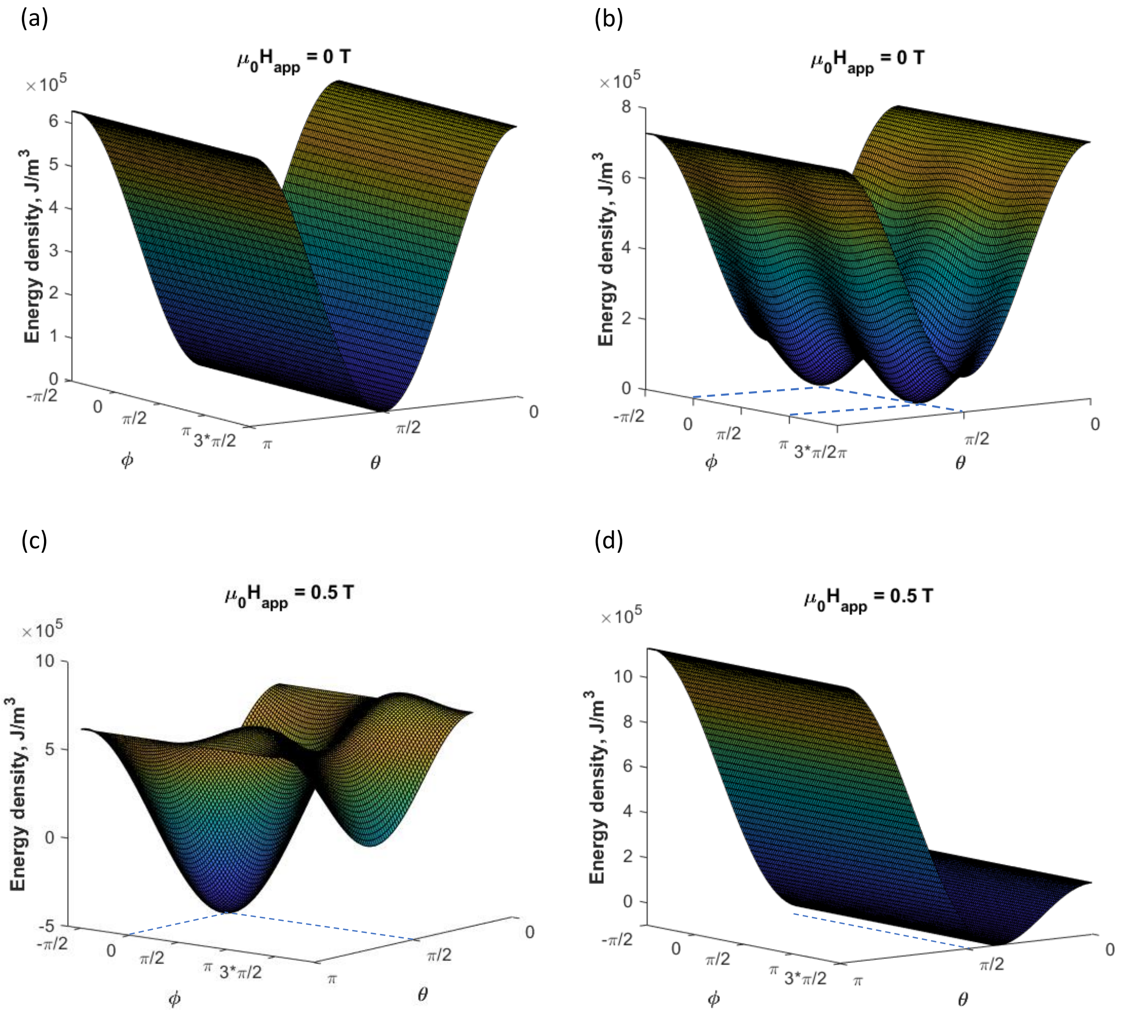

Fig. 4: Energy density of a thin film extended infinitely in the xy plane. This means N = (0,0,1). In (a) and (b) the external magnetic field is turned off for a better understanding of the effect of MCA; (a) is without and (b) with MCA. In (c) and (d) there is only the effect of the external field H_{app} in the positive x (c) and z (d) direction respectively for a thin film without MCA. Parameters:

	Ku//x	Ms	Happ
a	0	1e6 A/m	0
b	*1e5 J/m^3*	1e6 A/m	0
c	0	1e6 A/m	0.5T//x
d	0	1e6 A/m	0.5T//z

To better illustrate how the external magnetic field changes the energy landscape and the position of energy minima or maxima, figure 5 shows a cut along φ at θ = π /2, for conditions that are the same as in figure 4b. The field was applied in the direction of the easy axis, pointing towards the φ

= 0 direction. With no external field there are two identical minima in φ = 0 and φ = π, but upon increasing the field value, the minimum in φ = π becomes a maximum for a strong enough value of H_{app}. This will be important when considering the precession modes under spin transfer torque.

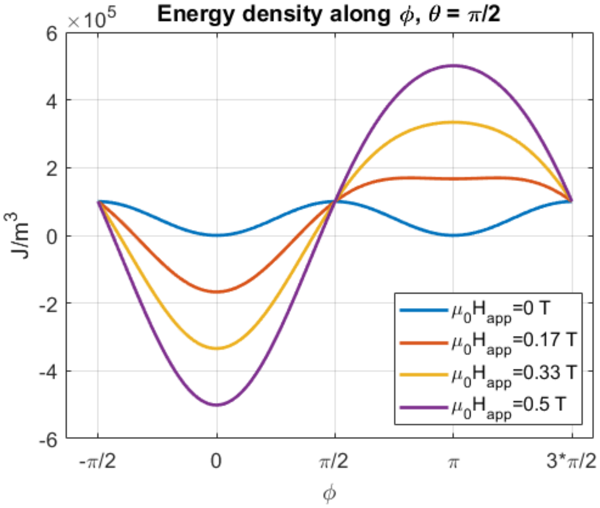

Fig. 5: Effect of the change of the external magnetic field on the energy density.

2.4.3 LLGS equation

The dynamics of the magnetization is governed by the **Landau-Lifshitz-Gilbert equation** (LLG equation) that corresponds to the first two terms in the right hand side of eq. 5. Moreover, when spin transfer torque is present, the third term, introduced by Slonczewski [7], is added to eq. 5, and the resulting expression is called **Landau-Lifshitz-Gilbert-Slonczewski equation** (LLGS equation),given in eq. 5, where γ_0 is equal to the product $\gamma\mu_0$, γ being the gyromagnetic ratio and μ_0 the permeability of free space. In eq. 5 a_j is the spin torque prefactor, that is dependent upon the current density ***J*** and hence the transversal area, the thickness of the magnetic layer *t,* and the spin polarization efficiency η.

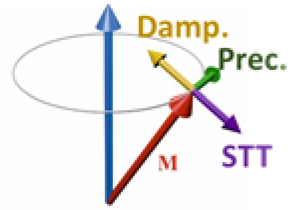

Fig. 6: depiction of the action of the different terms in the LLGS equation.

The terms in eq 5. correspond, from left to right, to the precession, damping and spin transfer torque. Their action on the magnetization is depicted in figure 6 and each one of them will be explained in the following sections.

$$\frac{\partial \boldsymbol{M}}{\partial t} = -\gamma_0\left(\boldsymbol{M}\times\boldsymbol{H}_{eff}\right) + \frac{\alpha}{M_s}\left(\boldsymbol{M}\times\frac{\partial \boldsymbol{M}}{\partial t}\right) + \gamma_0\frac{a_j}{M_s}[\boldsymbol{M}\times(\boldsymbol{M}\times\boldsymbol{P})],$$

$$with\ a_j = \frac{\hbar}{2e}\frac{\eta}{\mu_0 M_s t}\boldsymbol{J} \qquad (5)$$

2.4.4 Conservative dynamics

Equation 6 is the **conservative dynamics** version of eq. 5 where just the first term (precession term) is taken into account.

$$\frac{\partial \boldsymbol{M}}{\partial t} = -\gamma_0 \left(\boldsymbol{M} \times \boldsymbol{H}_{eff} \right) \qquad (6)$$

Conservative means that the trajectories described by eq. 6 keep a constant energy. Indeed, the change of energy density in time (eq. 7a), is like performing a dot product of eq. 6 with H_{eff} (eq. 7b) and this is zero.

$$\frac{\partial E_{density}}{\partial t} = \frac{\partial E_{density}}{\partial \boldsymbol{M}} \frac{\partial \boldsymbol{M}}{\partial t} \qquad (7a)$$

$$-\boldsymbol{H}_{\boldsymbol{eff}} \frac{\partial \boldsymbol{M}}{\partial t} = 0 \qquad (7b)$$

In the second place, from eq. 6 one can know that the static equilibrium of the magnetization $\left(\frac{\partial \boldsymbol{M}}{\partial t} = 0 \right)$ happens when both **M** and $\mathbf{H}_{\mathbf{eff}}$ point in the same direction, as mentioned before in the discussion about the effective field in 2.4.2.

Furthermore, the time derivative of the squared norm of **M** is zero, as eq. 8 shows and this implies that the magnitude of **M** is constant. This is always the case for a ferromagnet.

$$\frac{\partial |\boldsymbol{M}|^2}{\partial t} = 2\boldsymbol{M} \, \frac{\partial \boldsymbol{M}}{\partial t} = 0 \qquad (8)$$

2.4.5 Dynamics with dissipation

The second term in the eq. 5 introduces the **dissipation of energy** where α is the damping constant; this magnetic damping was introduced by Gilbert and Kelly [8,9]. It attenuates the precessions until the system is brought back to the static equilibrium defined by $\frac{\partial \boldsymbol{M}}{\partial t} = 0$, which requires $\mathbf{H}_{\mathrm{eff}}$ and **M** to be parallel or equivalently that **M** is aligned along the energy minimum, as stated in section 2.4.2. Furthermore, the magnitude of **M** remains constant when this dissipation term is added to the precession term, because if one makes the dot product of the equation with **M**, the expression goes to zero as mentioned in the previous paragraph.

2.4.6 Linearization of LLG precession term

The LLG equation is difficult to solve analytically because of the non-linearity of its terms. For example, the conservative term is non-linear because $\mathbf{H}_{\mathbf{eff}}$ depends on the magnetization **M** due to the dipolar field. However, for small perturbations it is possible to make a linearization of **M** and $\mathbf{H}_{\mathbf{eff}}$ that provides the ferromagnetic resonance (FMR) mode and its frequency. This linearization is shown in equation 9 for spherical coordinates. For this and the following expressions *E* is the energy density, the subscripts θ and φ, indicate a partial derivative with respect to that variable, which can be single or double depending on the number of subscripts. The process is shown for conservative dynamics: the linearized expressions of 9 are substituted in eq. 6 and the equation 10a is obtained, where second order terms have been neglected. The following step assumes that $\delta m_\theta, \delta m_\varphi$ have the form $e^{i\omega t}$ and therefore $\delta\dot{m}_\theta, \delta\dot{m}_\varphi$ are proportional to $i\omega\delta m_\theta, i\omega\delta m_\varphi$; this allows us to write eq. 10b, from which the frequency can be calculated through the determinant that leads to eq. 11, this is the natural resonance frequency of the system.

$$\boldsymbol{M} = \boldsymbol{M_o} + \boldsymbol{\delta m} = M_s\begin{pmatrix}1\\0\\0\end{pmatrix} + \begin{pmatrix}0\\ \delta m_\theta\\ \delta m_\varphi\end{pmatrix} \qquad (9a)$$

$$\boldsymbol{H}_{eff} = \boldsymbol{H^o_{eff}} + \boldsymbol{h}_{eff} = -\frac{1}{M_s}\begin{pmatrix}0\\ E^o_\theta\\ \dfrac{E^o_\varphi}{sin\theta}\end{pmatrix} + \frac{\boldsymbol{\partial H}_{eff}}{\boldsymbol{\partial M}}\boldsymbol{\delta m} \qquad (9b)$$

$$\frac{d\boldsymbol{\delta m}}{dt} = -\gamma\left(\boldsymbol{\delta m}x\boldsymbol{H^o_{eff}} + \boldsymbol{M_o}x\boldsymbol{h}_{eff}\right) \qquad (10\text{a})$$

$$0 = \begin{pmatrix}\left(-\dfrac{E_{\varphi\theta}}{M_s sin\theta} - i\dfrac{\omega}{\gamma}\right) & -\dfrac{E_{\varphi\varphi}}{M_s sin^2\theta}\\ \dfrac{E_{\theta\theta}}{M_s} & \left(\dfrac{E_{\theta\varphi}}{M_s sin\theta} - i\dfrac{\omega}{\gamma}\right)\end{pmatrix}\begin{pmatrix}\delta m_\theta\\ \delta m_\varphi\end{pmatrix} \qquad (10b)$$

$$\left(\frac{\omega_o}{\gamma}\right)^2 = \frac{E_{\theta\theta}E_{\varphi\varphi} - E^2_{\varphi\theta}}{M^2_s sin^2\theta} \qquad (11)$$

As can be noted from eq. 11, by means of the energy, the natural frequency depends on the specific structure of the free layer. Figure 7 depicts this frequency for the case of a magnetic layer with magnetocrystalline anisotropy along the x-axis and whose in-plane dimensions are much larger than the thickness in z, so that N_{zz} is approximately 1 for the analytical computations; the calculations are done for two different external field orientations. When H_{app} is applied in the in-plane direction, the formula of the frequency is eq 12a; when H_{app} is applied out of plane, there are two regimes: eq. 12b when the field is not strong enough to take the magnetization out of plane, i.e. H_{app} is less than the saturation field, and eq. 12c when H_{app} is larger than the saturation field. The expressions were derived from eq. 11 by taking the corresponding derivatives of the energy density for each field orientation. Besides, the numerical results are obtained from the LLG equation. From Fig. 7 it can be seen, that when the magnetization is aligned with the field (in-plane or put-of-plane), the frequency increases with the field. For the out-of-plane field configuration, when H_{app} is less than the saturation field, the frequency decreases and goes to zero when H_{app} is equal to the saturation field. These are typical frequency-field dispersions.

$$\omega_0 = \gamma_0\sqrt{(-H_d + H_{app} + H_{anis})(H_{app} + H_{anis})} \qquad (12a)$$

$$\omega_0 = \gamma_0 \sqrt{-H_u(H_d - H_{anis})\left[1 - \left(\frac{H_{app}}{H_d - H_{anis}}\right)^2\right]} \qquad (12b)$$

$$\omega_0 = \gamma_0 \sqrt{(H_{app} + H_d - H_{anis})(H_{app} + H_d)} \qquad (12c)$$

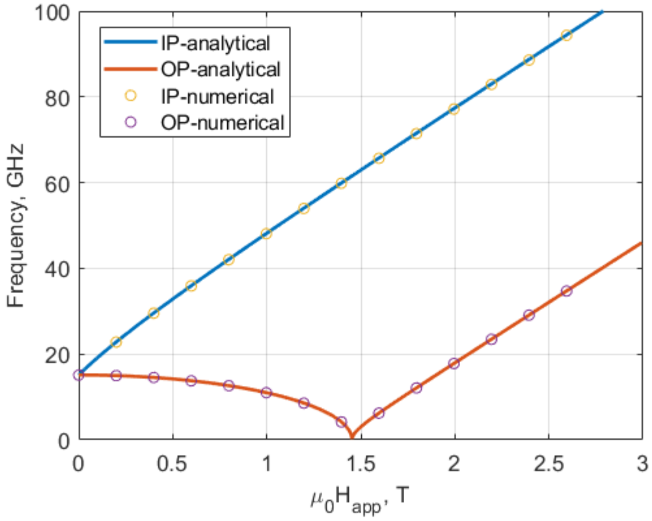

Fig 7: Frequency f_o for different orientations of the external magnetic field: In-Plane (IP) or xy plane and Out of Plane (OP) or along z axis. M_s=1e6 (A/m), K_u=1e5 (J/m3), α=1e-5, 1e5x1e5x3 nm.

2.4.7 STT driven magnetization dynamics

For simplicity, the effect of the STT will be illustrated for a free layer with both the magnetocrystalline anisotropy and the magnetic field oriented in the in-plane direction.

Static state. When a spin polarized current is injected through the ferromagnetic layer, the third term of the LLGS equation 5, that is the spin transfer torque (STT) term, has to be taken into account**.** There are two basic configurations of the polarizer: the planar one (figure 8a), and the perpendicular polarizer (figure 8b). In the first case, the polarization **P** is collinear to **H$_{\text{eff}}$**, that points in the direction of the energy minimum as mentioned before. Therefore, when **M** is aligned in the direction of the energy minimum, the precession torque and the spin transfer torque, which are the two terms in eq. 13, are zero and the condition for the static equilibrium is fulfilled for both terms independently. In the case of the perpendicular polarizer, **P** and **H$_{\text{eff}}$** are not parallel anymore. Thus, in the static equilibrium the precession torque and the spin torque are non-zero and define a new position of **M** where the two terms compensate each other. This involves a rotation of the magnetization in the in-plane direction, that corresponds to the xy plane. Moreover, this rotation will be larger if the current is increased [10], up to the critical angle φ_c and critical current J$_c$, which is the point where instability is reached and a transition to a dynamical state happens. This situation will be further illustrated and discussed in the results sections.

$$\gamma\big(\boldsymbol{M}\times \mu_0\boldsymbol{H}_{eff}\big)-\gamma\frac{a_j}{M_s}\big(\boldsymbol{M}\times(\boldsymbol{M}\times\boldsymbol{P})\big)=0 \qquad (13)$$

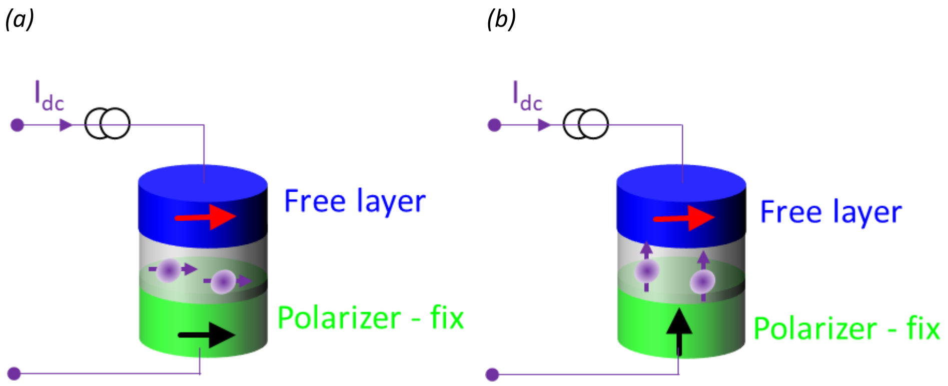

Fig. 8: Two basic configurations of the polarizer: the planar (a); the perpendicular (b).

Dynamic state. For small values of the injected current, the magnetization follows a damped motion, because the energy gained through spin torque compensates only partially the losses due to the natural damping. When the current is strong enough, at the critical current, J_c, the corresponding spin transfer torque balances the losses during one oscillation, and a limit cycle (a concept from non-linear dynamics) is established, that is characterized by stationary state oscillations. This state is maintained stable even when the spin torque overcomes the damping torque, because of the non-linearity of the LLG equation: these two torques depend on the amplitude of the precession of the magnetization.

Following a similar procedure of linearization of eq. 5 and the one employed for finding the natural frequency for the conservative case, section 2.4.6, the general complex frequency when including damping and STT terms is given by eq. 14, where ω_o is the natural frequency, $\Delta\omega_o$ is the linewidth, or in other words the Full Width at Half Maximum (FWHM) and P_r is the radial component of the polarization written in spherical coordinates. In this case, the frequency is complex: $\omega = \omega' + i\omega''$, where ω' gives the precession frequency, and $i\omega''$reflects the losses.

$$\left(\frac{\omega}{\gamma'}\right)=\frac{i}{2}\left[\frac{\Delta\omega_o}{\gamma}+2a_jP_r\right]\pm\sqrt{-\frac{1}{4}\left[\frac{\Delta\omega_o}{\gamma}+2a_jP_r\right]^2+(1+\alpha^2)\left[\left(\frac{\omega_o}{\gamma}\right)^2+\left(a_jP_r\right)^2\right]},$$

$$\gamma'=\frac{\gamma}{1+\alpha^2}\quad P_r'=P_x\sin(\theta_0)\cos(\varphi_0)+P_y\sin(\theta_0)\sin(\varphi_0)+P_z\,cos(\theta_0) \qquad (14)$$

From eq. 14, it is possible to derive the instability limit that allows the transition from a static to a dynamic state, and hence one can find the critical current. This transition requires ω'', the imaginary part of ω, to be zero, which is accomplished differently for different structures. For our device and considering a perpendicular polarizer, since the direction of the polarization **P** has only a component in the θ direction, its radial component P_r' is zero. Therefore, for ω'' to be zero, it is necessary that

ω_o is zero. These conditions are satisfied for a critical angle and a critical current given by eq. 15a and eq. 15b respectively. In the case of a planar polarizer, the critical current requires the term under square root to be real and the imaginary part outside the radical to be zero, this leads to eq. 15c.

$$\varphi_c = -\frac{H_{app}}{2H_u} \pm \sqrt{\left(\frac{H_{app}}{2H_u}\right)^2 + 0.5} \qquad (15a)$$

$$\boldsymbol{J_c} = \frac{2e}{\hbar}\frac{M_s t}{g(\eta)} \times \left(H_u \sin(\varphi_c)\cos(\varphi_c) + H_b \sin(\varphi_c)\right) \qquad (15b)$$

$$\boldsymbol{J_c} = -\alpha\left(2H_{app} + 2H_u - H_d\right)\frac{e\mu_0 M_s t}{\eta\hbar P_r} \qquad (15c)$$

2.4.8 Magnetization trajectories under STT

The trajectories followed by the magnetization when the limit cycle is reached depend on the type of polarizer employed. Let us first start with the planar polarizer. When the limit cycle is reached, IPP (In-Plane Precession) takes place which is a precession around the energy minimum, figure 9a. If the current is increased, two different scenarios can occur: the first one is when $\mathbf{H_{app}} < \mathbf{H_{anis}}$; in this case, the energy density follows a shape similar to the blue and red curves in figure 5 where $\varphi = \pi$ is still a local energy minimum. Hence, when the current is large enough, and it provides to the system an energy greater than the saddle point (which corresponds to $\varphi = \frac{\pi}{2}$ in figure 5) the magnetization shifts from precessions around the minimum in $\varphi = 0$ to a state of damped precessions around $\varphi = \pi$. In the second scenario $\mathbf{H_{app}} > \mathbf{H_{anis}}$ and $\varphi = \pi$ is not a minimum anymore as shown for the yellow and purple curves in figure 5. Then, when the current is large enough to provide an energy that overcomes the saddle point, the magnetization goes to the OPP mode (figure 9b).

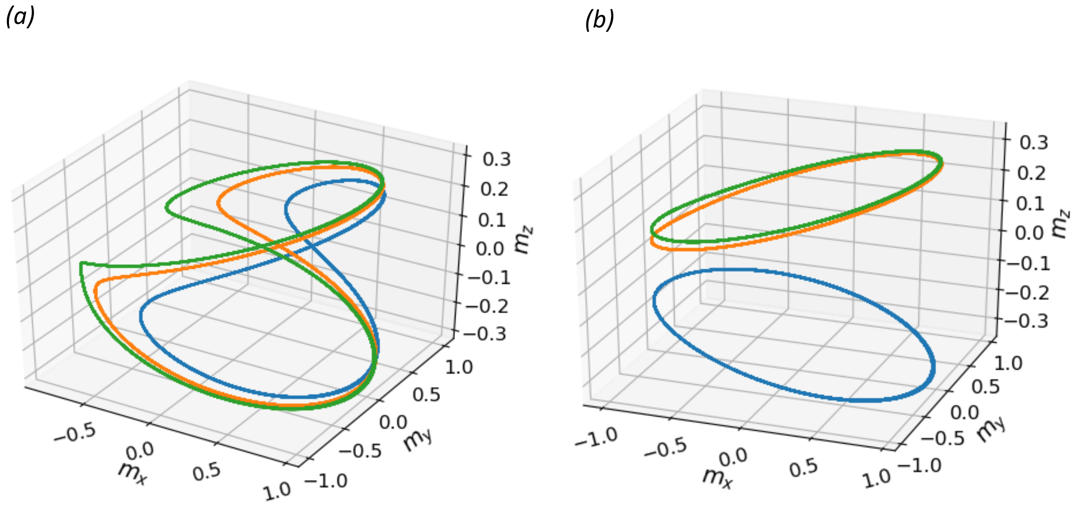

*Fig. 9: Precession modes. Free layer of 100x100x3 nm^2. M_s=1e6 (A/m), K_u=1.5e3 (J/m3), $\mu_0 H_{app}$=0.03 T, α=0.01, **p**=(1,0,0). (a) represents an In-Plane Precession mode (IPP). (b) shows an Out of Plane Precession mode (OPP).*

For the perpendicular polarizer, since the spin torque is already taking the magnetization in the out of plane direction, there is a direct transition from the static in-plane state to the OPP trajectory. The transition, as pointed out before, happens when the static in-plane rotation of the magnetization reaches a critical angle which corresponds to the moment when STT term overcomes the precession term.

The OPP mode is of great interest for synchronization, because of its larger amplitudes of precession compared to those of IPP mode, which allows for a better dipolar coupling between oscillators. Furthermore, the circular symmetry of this mode, in contrast to the ellipsoidal one of the IPP mode, simplifies the mathematical treatment of the dynamics of these trajectories. This is why we chose a system that stabilizes such OPP modes. It should be mentioned that the perpendicular polarizer was chosen for this thesis, because with respect to the planar polarizer it makes easier the generation of OPP modes.

2.4.9 Non-linearity of STNOs

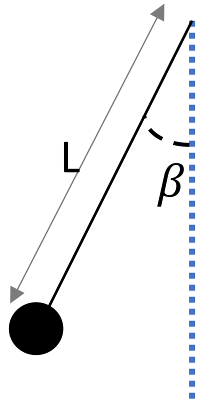

Fig 10. Single pendulum

A feature that is particular to STNOs is the non-linearity of the precession term in eq. 5, or in other words, the dependence of the frequency on the amplitude of oscillations. To illustrate this, one may recall the example of a simpler system: a single pendulum (figure 10). For small oscillations, the angular frequency can be expressed by eq. 16a, which is independent of the amplitude. Nevertheless, when larger oscillations are considered, the angular frequency depends on the angle β_0 and hence on the amplitude (eq. 16b).

$$\omega_0 = \sqrt{\frac{g}{L}} \quad (16a)$$

$$\omega = \omega_0 + k\beta_0 \quad (16b)$$

In the case of STNOs, one can obtain an expression of the frequency with respect to the oscillation power *p*, which is related to the amplitude (eq. 17) [11]. This opens the possibility to use a current that through the STT term in the LLGS equation is able to change the oscillation amplitude and hence the frequency of the STNO.

$$\omega = \omega_0 + Np \qquad (17)$$

In eq. 17 *N* is the non-linear frequency shift coefficient.

3. Modelling

The objective of this project is to study the dynamical state of a single and a set of coupled spin torque nano-oscillators (STNO). The dynamics of the magnetization and the coupling between oscillators depend on different parameters: the dimensions of each oscillator, the separation between them, the type of coupling that can be via current or via field, the geometrical arrangement of the devices and external parameters like the applied magnetic field and the injected current. Two of these devices are depicted in figure 11.

As mentioned before here we consider only STNO structures with a perpendicular polarizer and an in-plane free layer. This structure has previously been studied at SPINTEC under in-plane field [10]. However such a field breaks the symmetry with respect to the out of plane direction. Therefore, we consider here the dynamics under field conditions that do not break this symmetry. This is an out of plane field. Since the conditions under which oscillations occur in this case were unknown, I performed first a detailed study for a single STNO.

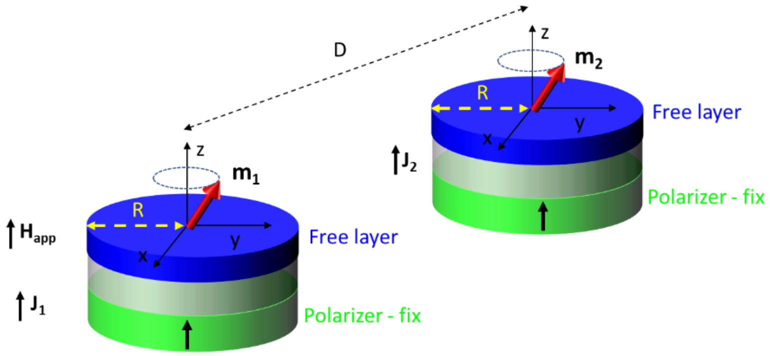

Fig. 11: Two identical STNO at a distance D, with radius R, applied field ***H_{app}****, current density* ***J*** *and magnetization of the free layer* ***m.***

In the following subsections, the code used throughout this work for the simulations is described.

3.1 Description of the code

As was mentioned in the previous section the LLGS equation governs the dynamics of the magnetization of the free layer in the presence of STT. Figure 12 presents the working scheme of the code provided by SPINTEC and that was used for integrating the LLGS equation. In this scheme, the voltage is used instead of the current density which has been mentioned in the previous section; both parameters are connected via Ohm’s law. The block called *initialisation* represents the reading from an input file of: the parameters of each layer of the MTJ such as thickness, radius, saturation magnetization and anisotropy; the simulation time step that was 5 ps, the time limit of the simulation, which was 100 ns, the time between saved points (those that will be saved in an output file), that was changed according to the precession frequencies involved, and the external parameters which are the applied magnetic field and the voltage intervals.

For the integration of the LLG equation, that is solved for each time step, there are three loops in the code: the inner loop is over the time advancing the time step until the time limit is reached; this is done for each pair of values of applied magnetic field and voltage. When the time loop is finished, the applied magnetic field is advanced by one step, this corresponds to the second loop; when the last field value is attained, the voltage is advanced by one step which corresponds to the third loop. The process finishes when the code arrives to the last values of the magnetic field and voltage.

It is noted that the magnetic field was applied with a finite rise time (1 ns) at the start of the time loop and the voltage was applied after ten nanoseconds with a finite risetime (1 ns) as can be seen from figure 13. This is done in this way because it corresponds to the manner in which the real experiments are performed: with a non-zero rise time and a magnetization that reaches the static equilibrium before undergoing the spin transfer torque.

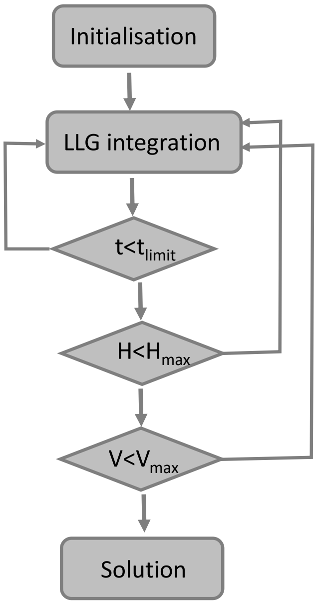

Fig. 12: Flow chart of the LLG solver.

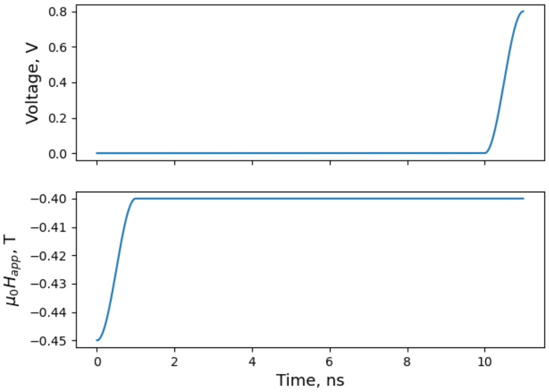

Fig. 13: Example of how the voltage and field excitations are applied.

For each value of voltage and magnetic field, when the simulation has been performed up to the time limit, the time traces of $m_x(t)$, $m_y(t)$ and $m_z(t)$ are saved in an output file for further processing, together with the evolution of the field and voltage. Two examples for the evolution of the three components of the magnetization through the transient and the stationary states are given in figures 14a and 14b. In the figure 14a, the final state is a static state, which means that after the transient, the system converges to a stable point. In the example this is an out of plane state. In figure 14b, a dynamic state is shown, where the magnetization performs oscillations with constant amplitude after the transient. In the example this is an OPP oscillation, for which m_x and m_y oscillate while m_z is constant.

This data is then analyzed through a Python code that I wrote for finding the frequencies of oscillation with the Fourier Transform and for plotting stationary state trajectories, time traces and state diagrams.

Although the simulation time limit is 100 ns, the Fourier Transform is made for a smaller interval of time where the magnetization is in a steady state. Since this time was chosen to be of 40 ns, the frequency resolution of the results is of 25 MHz, which is fine enough since the STNO generates a signal in the GHz range. Additionally, for each voltage and field step, one has the possibility to take as the initial magnetization some pre-defined values or the final state values from the previous step. This last possibility is necessary when one wants to take into account hysteresis effects.

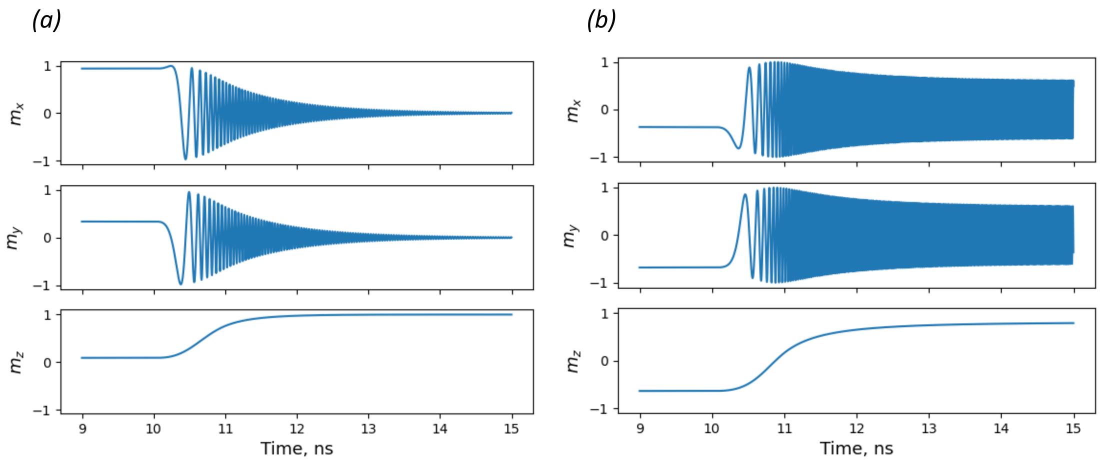

Fig. 14: Time traces of the magnetization components for a different pair of voltage and magnetic field. (a) indicate a static state. (b) is a dynamic state.

3.2 Description of the STNO structure

The structure studied in this thesis for the free layer involves a perpendicular polarizer and an external magnetic field oriented out of plane, figure 15a. The selection of the perpendicular field is motivated by the fact, that it keeps the symmetry of the OOP mode. This magnetic field can be implemented experimentally using a biasing magnetic layer via dipolar or exchange coupling.

While the real STNO structures have circular or elliptical cross sections Fig. 15b, within the LLG simulation the corresponding demagnetization field is approximated using a rectangular MTJ cross section, figure 15c. However, the difference in the calculations for a rectangle structure and an ellipsoidal one with the same magnitude of the principal axes is small enough to be neglected for the purposes of this thesis.

Different dimensions of MTJs were considered: first symmetric (circular) elements with the same length a=b in the x and y direction; thereafter asymmetric (elliptical) elements with different lengths a≠b in the x and y direction. This asymmetry changes the demagnetizing field because it is affected by the shape as already explained and induces an effective in-plane uniaxial anisotropy.

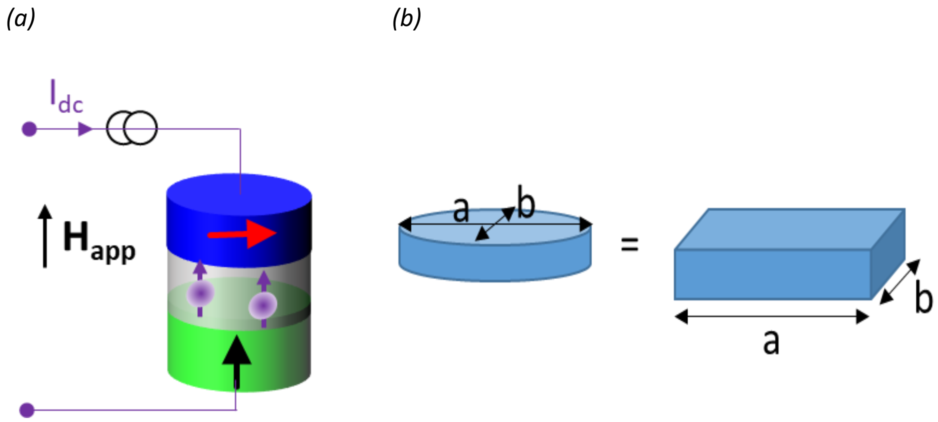

Fig. 15*: ellipsoidal structure (a) and its rectangular equivalent (b)*

The table 1 lists some of the physical parameters used in the simulations. Moreover, the spacer and the polarizer have a thickness of 1 and 2 nm respectively.

Parameter	**Free layer (M2)**	**Polarizer (M1)**
M_s (kA/m)	1000	1000
K_u (J/m^3)	0	4x10^6
u_K	(0,0,0)	(0,0,1)
Damping (α)	0.01	0.01
Sample T (K)	0	0
STT efficiency η	0.433	-
TMR	100	
R (Ohm)	300	

Table 1

4. Study of a single STO

This section describes the dynamic properties of a single STO of circular or elliptical cross section. From the simulation we first derive a state diagram that shows under which conditions of field and voltage a dynamic or static state is obtained. In the second place, the behavior of the frequency depending on the field and voltage is studied and 3D trajectories are used to illustrate some ideas. We also derive diagrams that depict the behavior of the angle θ and φ for the different states. Finally, the effect of hysteresis is studied comparing diagrams that were obtained under different simulation conditions.

4.1 Symmetric device

First, a free layer with dimensions 100nm x 100nm x 3nm was considered. Table 2 indicates some information about the simulation parameters used for this case. Additionally, since for voltages larger than 1 V, the period of precession was comparable to the time between saved points, it produced wrong results when the Fourier analysis was performed. Thus, this time was reduced to 2.5 ps.

There are other parameters specific to this symmetric STNO, that are listed in table 3.

Time step (fs)	Time between saved points (ps)	Applied voltage range (V)	Applied field range (T)
5	2.5 or 10	-1.5:1.5. Step: 0.2. Direction: (0,0,1)	-1:1. Step: 0.2. Direction: (0,0,1)

Table 2

Parameter	Value
$\mu_0 a_j$	15.834 mT/V
N_{xx}	0.029569
N_{yy}	0.029569
N_{zz}	0.918973

Table 3

4.1.1 Field-voltage state diagram

The results for these dimensions of the free layer are presented in figure 16, which is a Voltage-Field-Frequency diagram (VFH diagram). The frequency was calculated through the Fourier Transform of one of the magnetization components. Since the oscillations, as is shown below, are parallel to the xy plane, the m_x component was chosen. Furthermore, for each pair of values of applied voltage and external magnetic field, the magnetization started from the same initial conditions. In section 4.3we compare this case to diagrams calculated by using different initial conditions to study the effect of hysteresis.

Several regions can be identified in figure 16 associated to different static and dynamic states:

i) One region labeled as **OPP** corresponds to the condition for which the magnetization oscillates following stationary out of plane precessions (OPP) with different frequencies (circular trajectory from figure 17 with the 3D representation).

ii) The green line called **TS** (Tilted Static State) in figure 16 corresponds to the case when there is no STT effect (V = 0 V) on the magnetization and hence, without excitation, the system is in a static state. In this case, the magnetization has an angle θ that depends on the strength of the external magnetic field. As shown in Fig. 24 further below, starting, θ gradually decreases (increases) from θ =π/2 to θ =0 (π) for positive (negative) field. The field value when an angle 0 is reached is called the saturation field, which here has a value of B_{sat}=1.25T. This value is determined by the demagnetization field, $B_{sat}=\mu_o M_s$ and can be derived from energy minimization.

iii) The area surrounding the OPP regions corresponds to a static state wherein the magnetization is aligned with one of the energy maxima in $\theta = 0$ or $\theta = \pi$, that corresponds to the cases **OPS+** and **OPS-** respectively (depicted in figure 17).

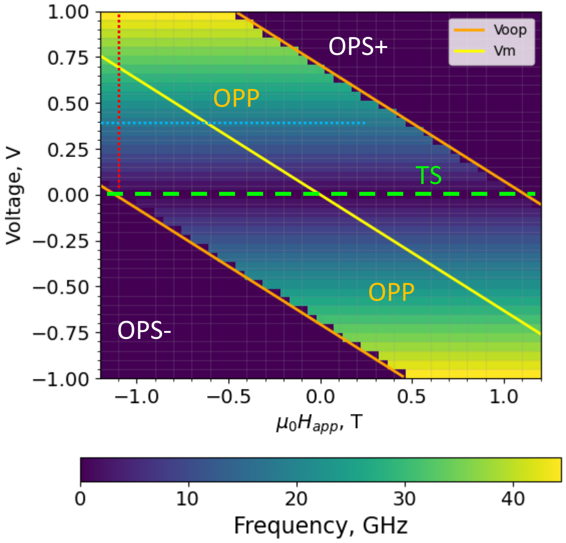

Fig. 16: VFH diagram for a Free layer of 100x100 nm^2. Parameters M_s=1e6, K_u=0, alpha=0.01, ***p****=(0,0,1). The applied field is out-of-plane. The red and blue dashed lines represent cuts along which the frequencies and trajectories were extracted to be plotted in figures 19 and 21*

The orange lines, in figure 16, in the transition to the OPS regions correspond to the out of plane voltage V_{oop}, that was computed analytically by a member of the RF group with eq. 18, where *t* and *A* are the thickness and the transversal area of the free layer respectively. V_{oop} is the voltage needed to take the magnetization to OPS+ or OPS-.

$$V_{oop} = -\alpha \frac{M_s}{a_{j0}} \left[\frac{H_{app}}{M_s} \pm \left(N_{zz} - \frac{N_{xx} + N_{yy}}{2} \right) \right],$$

$$where\ a_{j0} = \frac{\hbar}{2e} \frac{\eta}{\mu_0 M_s t R A} \qquad (18)$$

When a positive voltage is applied, a positive magnetic field H_{app} will support the voltage and hence V_{oop} will be smaller. On the other hand, a negative magnetic field will counteract the voltage and thus, V_{oop} will be larger. The same argument applies for a negative voltage: a negative field supports the voltage but a positive field counteracts it, which makes V_{oop}'s magnitude smaller and larger respectively. This is the reason of the slope of V_{oop}.

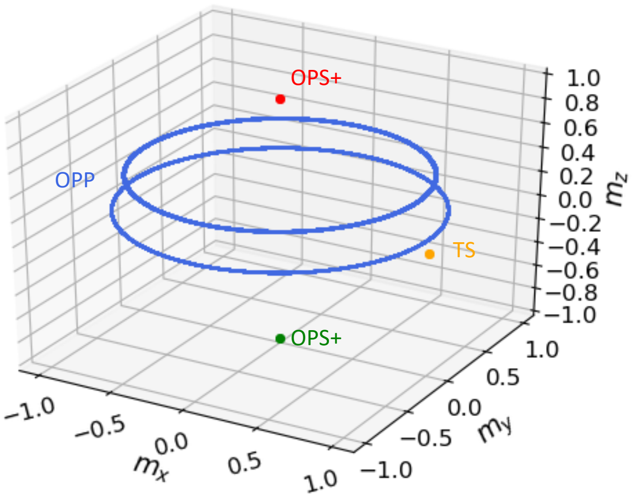

Fig. 17: Stationary state trajectories of the different regions of operation in the Field-Voltage state diagram.

4.1.2. Frequency dependence on the voltage

To illustrate the frequency dependence with voltage we take a cut along a constant value of H_{app} of the VFH diagram, represented by the red dashed line in figure 16. The frequency with respect to the voltage, figure 18a, along this cut exhibits a linear behavior and is in good agreement with the analytical formula eq. 19a computed by a member of the RF group. The difference of the computations with a numerical and an analytical approach is presented in figure 18b; the estimated difference is close to the resolution of the numerical calculations that is 25 MHz.

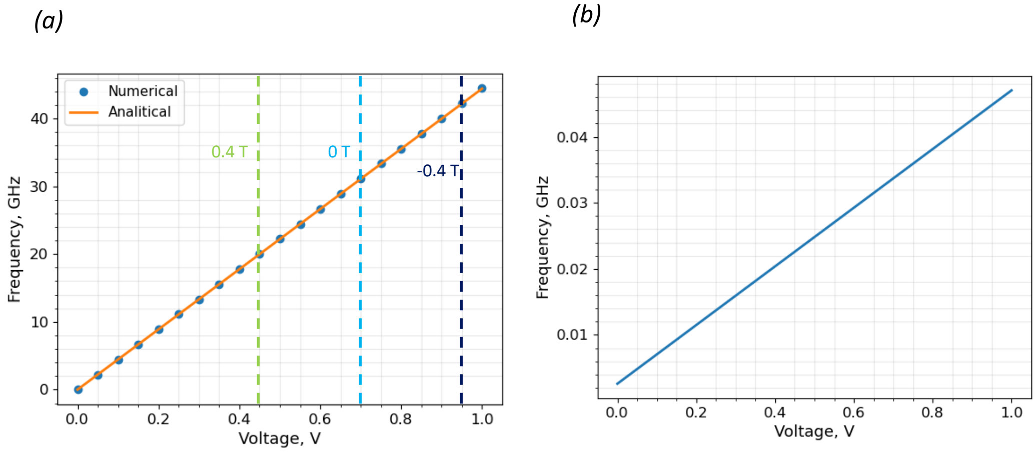

Fig. 18: Frequency vs Voltage. $\mu_0 H_{app}$ = -1.1 T. Numerical and analytical curves shown in (a), where the dashed lines correspond to the numerical value of V_{oop} for different fields. In (b) the differences of the results given by both curves is plotted.

$$f_{STO} = \frac{\gamma}{2\pi\alpha} a_j V \frac{N_{zz} - \frac{N_{xx} + N_{yy}}{2} - \frac{H_{app}}{M_s}}{\sqrt{\left(N_{zz} - N_{xx} - \frac{H_{app}}{M_s}\right)\left(N_{zz} - N_{yy} - \frac{H_{app}}{M_s}\right)}} \qquad (19a)$$

$$f_{STO} = \frac{\gamma}{2\pi\alpha} a_j V \qquad (19b)$$

Eq. 19a can be approximated to 19b when $N_{zz} \gg N_{xx}, N_{yy}$ or $N_{xx} = N_{yy}$. Eq. 19b exhibits a linear behavior as the numerical results showed in figure 18. Furthermore, with this approximation, the frequency becomes independent of H_{app} as will be discussed in the following section.

The 3D trajectories were also extracted, figure 19. From them the behavior of the amplitude of the precessions with respect to the voltage can be noted. The larger the voltage magnitude is, the more it pushes the magnetization towards one of the maxima, which in turn changes the magnitude of the oscillations. Since in the example of Fig. 19 the applied field is negative the oscillations start around m_z=-1. An important feature here is that upon increasing the voltage the m_z value decreases and becomes even positive.

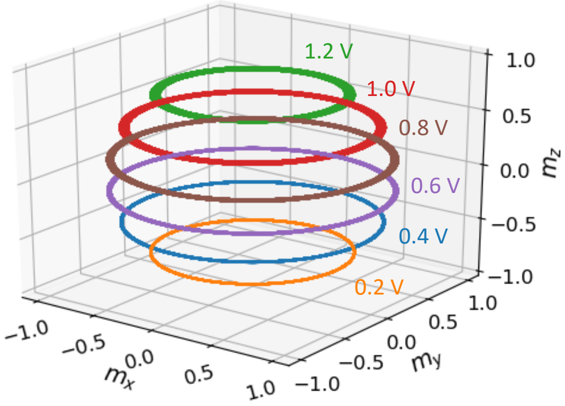

Fig. 19: Some 3D trajectories of the cut along $\mu_0 H$ = -1.1 T.

4.1.3. Frequency dependence on field

Another cut was made on the VFH diagram corresponding to the blue dashed line: a constant voltage of 0.4 V was defined and the data of the frequency with respect to different values of H_{app} were extracted, figure 20. A different behavior is observed: the frequency stays constant with respect to the external magnetic field; this result is expected from the analytical point of view, as eq 19b shows. Furthermore, the difference between the numerical and analytical results is close to the resolution of the numerical calculation of the frequency as evidenced in figure 20b.

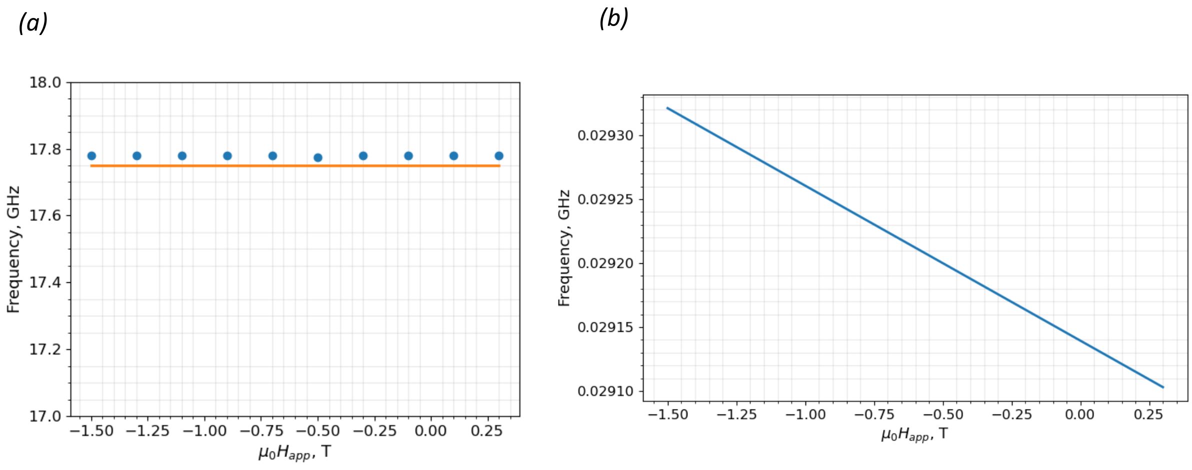

Fig. 20: Frequency vs $\mu_0 H_{app}$. V=0.4 V. Numerical and analytical curves shown in (a). In (b) the differences of the results given by both curves is plotted

On the other hand, this result is surprising because, as discussed before, the FMR frequency changes strongly with the magnetic field, that includes the contribution from H_{app} as figure 7 makes evident. In this case, where the Spin Transfer Torque comes into play, its effect on frequency compensates the change that is predicted by the FMR equations, and thus, at the end the frequency is kept constant.

Although the frequency is constant with respect to H_{app}, the amplitude of the oscillations is still changing, figure 21. Besides, since the dipolar field depends on this amplitude, and the coupling strength with nearest neighbors depends on the dipolar field, this behavior provides the possibility to tune the coupling strength with the external field keeping the frequency constant.

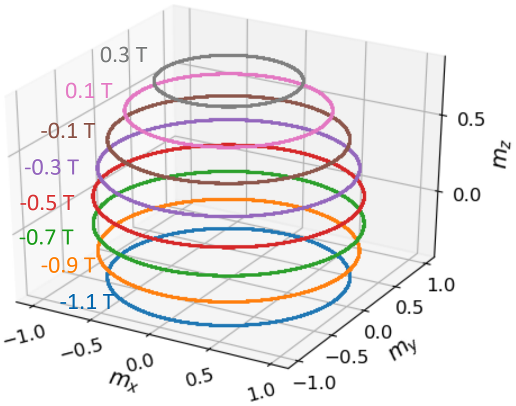

Fig. 21: 3D OPP trajectories at a constant voltage V = 0.4 V.

From figure 22 one can verify the already mentioned effect of the slope of V_{oop}, or in other words, the tilt of the OPP-OPS boundaries: for $\mu_0 H_{app}$ = 0.3 T a smaller voltage is needed to take the magnetization to the OPS+ state than in the case of $\mu_0 H_{app}$ = -0.3 T, because in the second situation the field is counteracting the effect of the voltage. In a complementary way and for the same reason, for $\mu_0 H_{app}$ = 0.3 T a larger negative voltage is needed to take the magnetization to the OPS- state than in the case of $\mu_0 H_{app}$ = -0.3 T.

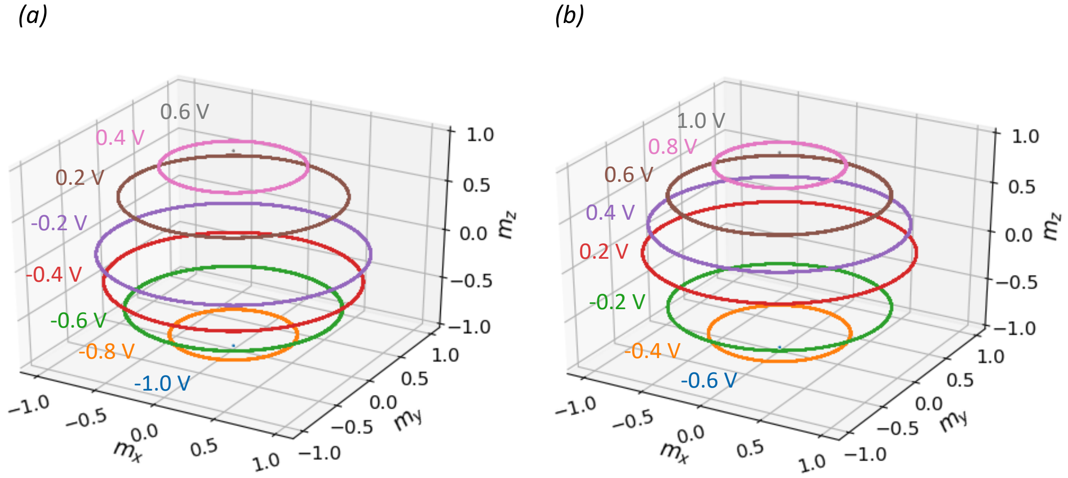

Figure 22: magnetization trajectories for different voltages and a constant external field. In (a) $\mu_0 H_{app} = -0.3\ T$*. In (b)* $\mu_0 H_{app} = 0.3\ T$*.*

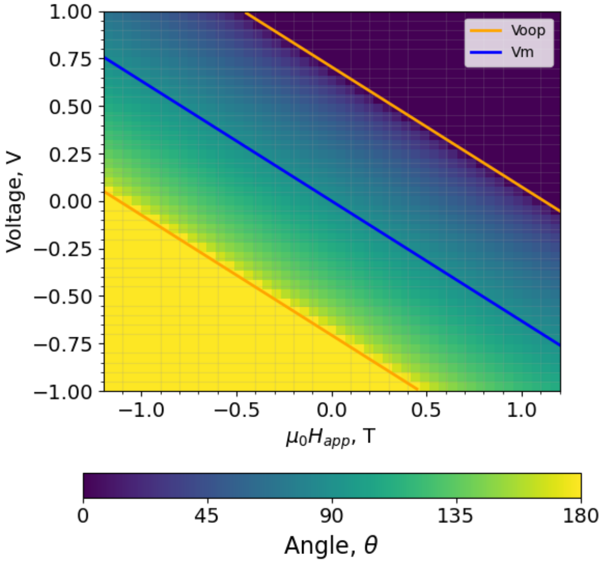

Fig. 23: Angle θ *diagram for a Free layer of 100x100 nm*^{2}*. Parameters* M_s*=1e6,* K_u*=0, alpha=0.01,* ***p****=(0,0,1). The applied field is out-of-plane.*

4.1.4. Polar angle θ diagram

The θ angle is a measure of the m_z component of the magnetization. Furthermore, from it one can estimate the amplitude of precessions which are smaller close to the angles $\theta = 0$ and $\theta = \pi$, and they are larger almost in the plane close to $\theta = \frac{\pi}{2}$. A diagram that shows θ in the stationary state for each value of voltage and H_{app} is shown in figure 23.

From the top right to the bottom left parts of the diagram, the θ angle reflects the transition of the magnetization from the OPS+ to the OPP and from the OPP to the OPS- states. For the dynamic states of OPP modes (within the V_{oop} boundaries) we can define a line (blue line), called V_m, given by eq. 20, that corresponds to the voltages and fields for which the dynamic angle θ is $\frac{\pi}{2}$ and the in-plan oscillation amplitude is maximum. Eq. 20 was obtained by a member of the RF group. Furthermore, the θ angle is constant for lines parallel to V_m and V_{oop}.

$$V_m = -\frac{\alpha}{a_{j0}} H_{app} \qquad (20)$$

For a fixed voltage, (including V = 0 V), the angle θ changes with H_{app} up to the moment when the static state OPS+ or OPS- is reached, this behavior is depicted in figure 24. The different curves in that figure have a similar behavior with respect to H_{app} and reach the static state for different magnetic fields.

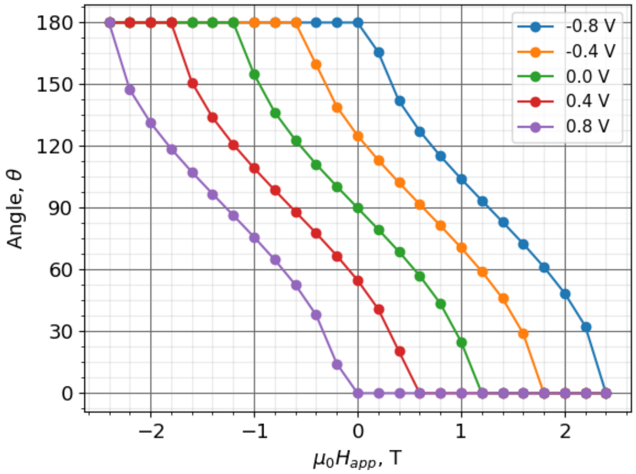

Fig. 24: The angle θ of the magnetization for different voltages and magnetic fields.

4.1.5 Simulation issues

It is important to point out that when the FMR frequencies of Fig. 7 were being evaluated numerically, an unexpected behavior was observed. As figure 25 indicates, when there was no external field or voltage applied, some oscillations appeared and grew in amplitude, instead of converging to a static state. For the calculation of the FMR frequencies small stable oscillations are needed around the static equilibrium points. Additionally, with the purpose of not having the oscillations attenuated, the damping coefficient was reduced several orders of magnitude. However, since the simulation time step was not decreased likewise, this error was produced. Finally, the damping coefficient was increased instead of decreasing the simulation step, so that the computation time would not be too long.

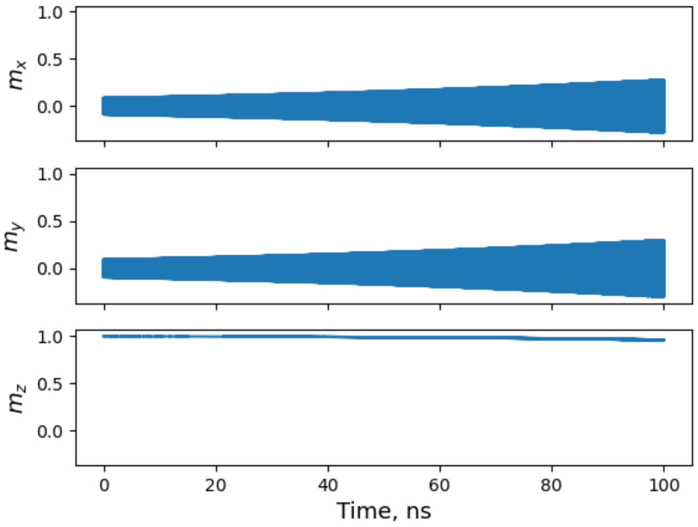

Fig. 25: Magnetization time traces. No voltage or external magnetic field is applied. Ms=1e6 (A/m), Ku=1e5 (J/m3), α=1e-5, 1e5x1e5x3 nm.

4.2. Asymmetric device

The motivation for the study of the elliptical or asymmetric device is to check the role of the shape anisotropy on the dynamics of the magnetization. The same diagrams that were used to study the circular device are used here to understand the differences in the behavior that arise.

The dimensions of the free layer were (130x100x3) nm ; the thickness of the polarizer and the spacer were 2 and 1 nm respectively. Table 4 and 5 indicate some information about the parameters used for this case.

Time step (fs)	Time between saved points (ps)	Applied voltage range (V)	Applied field range (T)
5	10	-1.0:1.0. Step: 0.05. Direction: (0,0,1)	-1.2:1.2. Step: 0.05. Direction: (0,0,1)

Table 4

Parameter	Value
$\mu_0 a_j$	12.18 mT/V
N_{xx}	0.023229
N_{yy}	0.030473
N_{zz}	0.946298

Table 5

4.2.1. Voltage–field state diagram

Noticeable differences are expected with respect to the previous case, because now, due to the changes in the shape of the device, the components of the demagnetization tensor change as table 5 indicates. N_{xx} and N_{yy} are not equal anymore as in the symmetric device and therefore, the dipolar interaction introduces an energy minimum in the in-plane x-direction. The effect that this has on the energy is similar to what happens when magnetocrystalline anisotropy is introduced, figure 4, as was seen in section 2.4.1. For the symmetric device, there was not a preferred in-plane direction, as in figure 4a, hence, the energy was the same for every possible φ angle when **m** was in-plane oriented ($\theta = \frac{\pi}{2}$). In that case, for any amount of energy injected to the system through a spin polarized current, **m** will go out of plane. Nevertheless, when there is an asymmetric shape, as in figure 4b, **m** will rotate to a new static state if a voltage is applied, similarly to the case discussed in section 2.4.7. The in-plane rotation angle has been extracted and is discussed in context of Fig. 32.

The VFH diagram is shown in figure 26b. The most noticeable difference with respect to the symmetric case is that the part of the diagram corresponding to TS is enlarged. This is a consequence of what was mentioned in the previous paragraph: there is an in-plane rotation of the magnetization towards a new static state before it goes to OPP. Additionally, in the diagram, there are two lines called V_{stat} that were calculated through eq. 21 by a colleague of the RF group, and they represent the threshold voltage for changing from TS to OPP. Eq. 21 can be derived from the static solutions of the LLG equation written in θ, φ coordinates.

$$V_{stat} = \pm \frac{M_s}{a_{j0}} \frac{N_{yy} - N_{xx}}{2} \qquad (21)$$

In figure 26a V_{oop}, V_m, V_{stat} were calculated with the parameters of the symmetric oscillator for making evident the effect that a change in the dimensions of the device can exert on the dynamics of the magnetization: : the three voltages have changed, firstly, because of the change of the coefficient $a_{\mathrm{j}0}$ that depends directly on the cross section area. In the second place, V_{stat}, in figure 26a is a single line along V = 0 V, which reflects the fact that for the symmetric device, any voltage can take the magnetization to a dynamic OPP state. Moreover, the width of the OPP region, or equivalently, the distance between the two lines of the V_{oop} is enlarged because of the dependence of this function on N_{zz}, that is bigger for the asymmetric case.

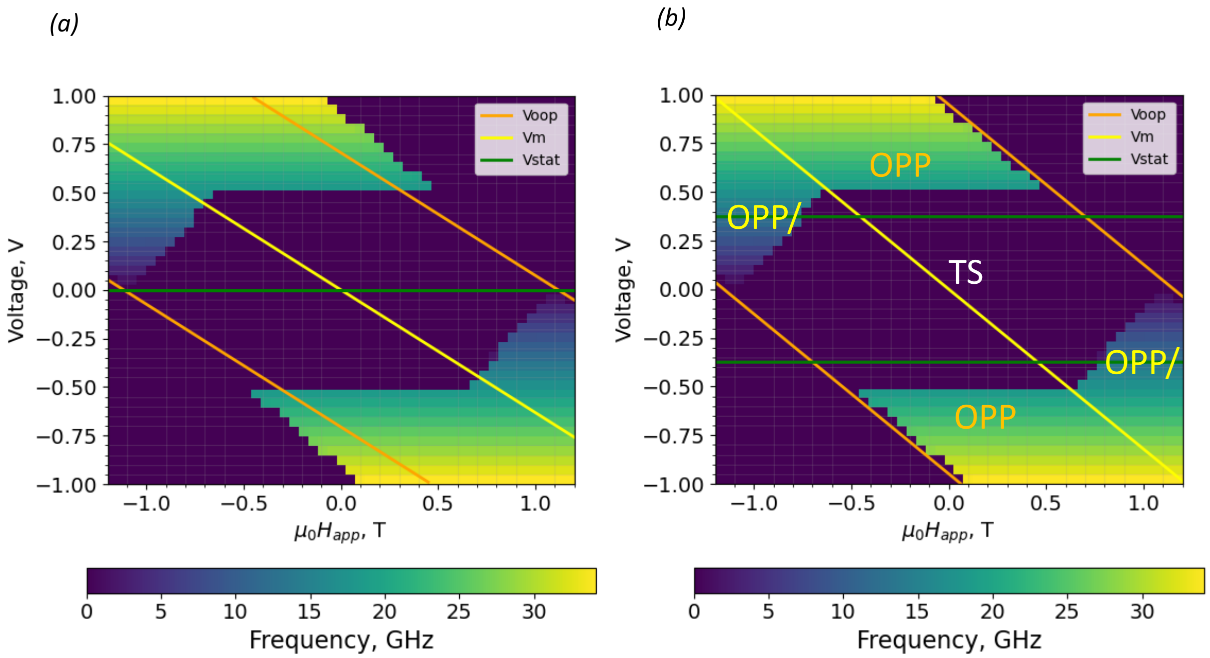

Fig. 26. VFH diagram for a Free layer of 130x100 nm^2. Parameters M_s=1e6, K_u=0, alpha=0.01, ***p****=(0,0,1). The applied field is out-of-plane. In (a) the curves of V_{oop}, V_m and V_{stat} were calculated with the values from the symmetric device and in (b) with the correct ones, for making clear the changes in the shape of the diagram.*

Besides, within OPP, there are two triangular sub-regions called **OPP/**, that indicate a gradual decreasing of the required voltage for going to OPP from the static state. This is because $\mathbf{H}_{\mathbf{app}}$, that pushes **M** out of plane, starts to be significant with respect to the dipolar field $\mathbf{H}_{\mathbf{d}}$, that pushes **M** in-plane. Therefore, the energy required to start out of plane precessions decreases.

Figure 27 plots the frequency with respect to the voltage at a constant external field for the STNO discussed so far. A comparison between them leads one to the conclusion that, with respect to the symmetric device, the frequency decreased for the same voltages for this asymmetric case. This is not surprising, because as eq. 19a indicates, the frequency is proportional to the prefactor a_j that is inversely proportional to the area of the device.

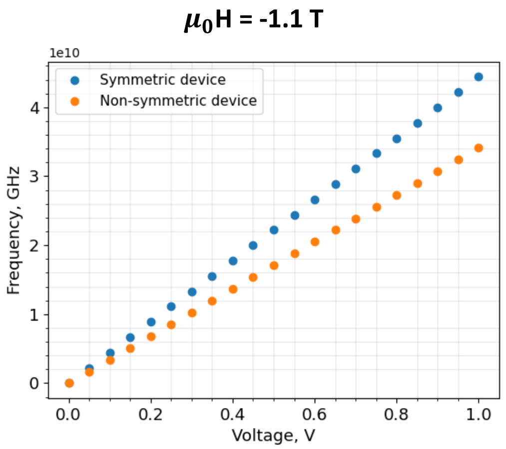

Fig. 27: frequency of precessions with respect to voltage. $\mu_0 H_{app}$ = -1.1 T.

The way in which different fields affect the behavior of the oscillations for a certain range of voltages, depicted in figure 28, makes evident the presence of the TS region, because there are some voltages that do not trigger a dynamical state and hence no trajectory is drawn for them in the plots. This contrasts with figure 22, where there is always a stationary state precession through the range of voltage considered. On the other hand, it is verified that a negative field supports a negative voltage and thus they lead the magnetization to the OPS- state at a lower voltage, with respect to the case of a positive magnetic field.

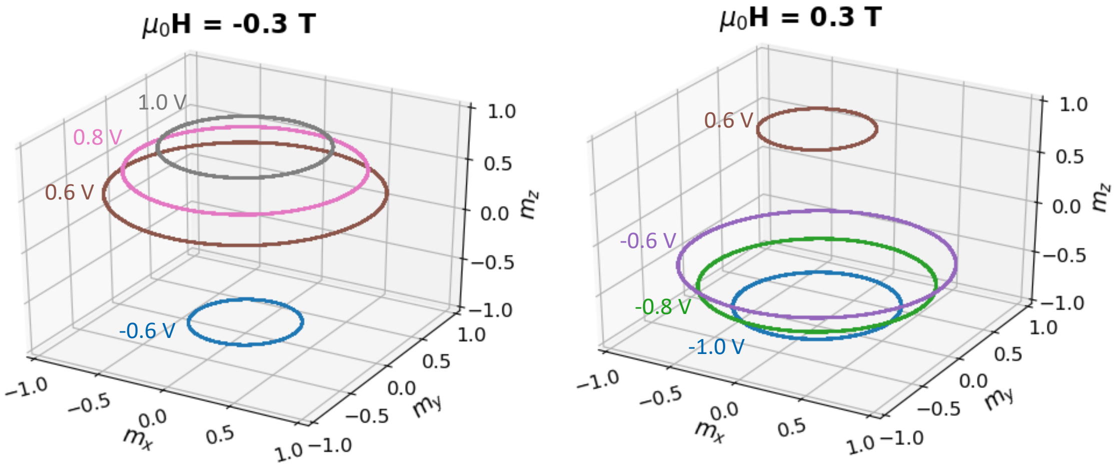
(a) External field = -0.3 T

(b) External field = 0.3 T

Fig. 28: magnetization trajectories for a range of voltage between -1 V and 1 V. The "missing" trajectories correspond to static states. Non symmetric structure.

4.2.2. V_{stat} verification

A notorious feature from the diagram in figure 26b is the disagreement between the result from the analytical expression of V_{stat} and the numerical outcome. The analytical value is 0.374 V and the numerical one is 0.55 V which gives a difference of 47 %.

The effect of hysteresis was evaluated to see if it was behind the reason of the disagreement. Hence, for some values of H_{app}, an increasing and decreasing sweep of voltages was evaluated, without resetting the magnetization position. An example of the way in which the external input parameters (H_{app} and V) were imposed is given in figure 29, where each curve represents the voltage applied to the STNO in each time trace simulation.

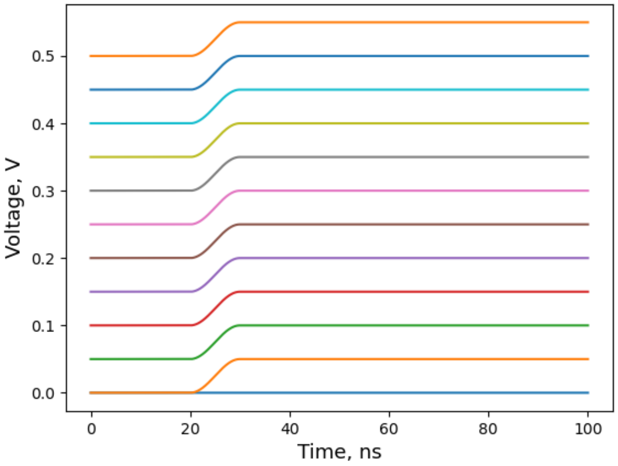

Fig. 29: Sweep of applied voltage at $\mu_0 H_{app}$ = 0.2 T. For each time trace the voltage starts from its previous value and then it is increased.

The results from the simulations, evidence that hysteresis does affect the boundary between the dynamic and static states, so that this threshold value is different when sweeping the voltage up, figure 30a, or sweeping down, figure 30b. In the former situation it is 0.55 V and in the latter 0.05 V, but both are still quite far from the analytical value of V_{stat}.

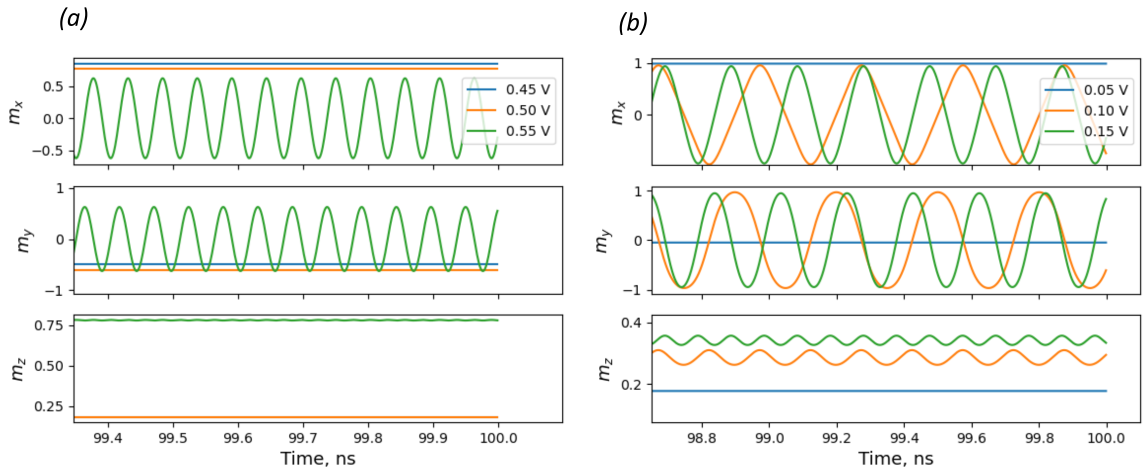

Fig. 30. Hysteresis effect simulation of the transition between the –IPS- state and the OPP state. Voltage weeps at 0.2 T (a) shows a sweep up from the TS to the OPP regions. In (b) a voltage sweep down was made from the OPP to the TS region.

4.2.3. *2f_{STO}* frequency

The asymmetry induced by the shape anisotropy causes the magnetization to energetically prefer the larger dimension direction in the static state (in absence of STT), as mentioned above. Besides, the precession torque in the LLGS equation (eq. 5) changes depending on the magnetization direction during its oscillation: when **M** and **H_{eff}** are parallel this torque is zero, but if they are perpendicular it is maximum. This results in a change in the shape of the 3D trajectory, that in the frequency domain can be seen as the introduction of a $2f_{STO}$ component in m_z. f_{STO} is the fundamental frequency of the oscillator at a certain voltage. Figure 31a, shows the frequency of m_x, m_y and m_z components.

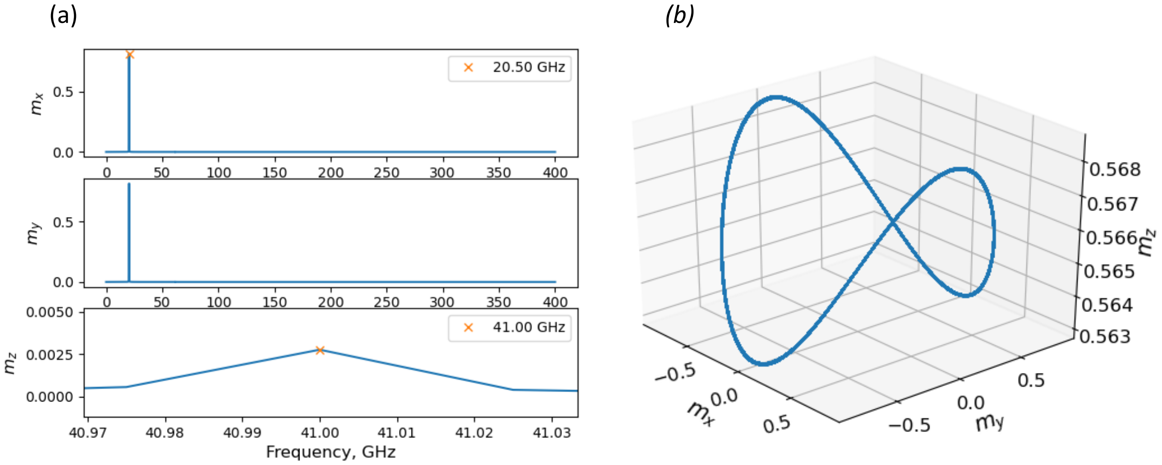

Fig. 31. Frequency components in the asymmetric STNO. The FFT is shown in (a). Besides, the 3D trajectory of the magnetization is plotted in (b).

4.2.4. Polar angle θ and azimuthal angle φ diagrams

The features and different regions seen in the VFH diagram, can also be distinguished in the angle θ and angle φ diagrams, figure 32. For the TS region, both θ and ϕ are defined because it corresponds to a static state and hence the angles are not time dependent; in the OPP region only θ can be considered constant because its variations are rather small (figure 31b), but φ is oscillating, thus, only θ is defined; in the OPS regions, since θ is equal to zero or π, φ does not have a particular value, it is not defined.

A difference that can be pointed out with respect to the VFH diagram is that the TS region expands beyond the limits given by the analytical value for the V_{oop} curve. This effect still has to be understood.

Furthermore, the lines of constant θ parallel to V_m that were continuous in the symmetric case, figure 23, now are interrupted in the TS static state region, where this angle behaves differently. In other words, there is a discontinuity in θ that appears in the transition between OPP and TS, which can be observed in figure 33 for the curves corresponding to -0.4 and 0.4 V. This is because of the dynamical differences between the regions: in TS the magnetization rotates towards a static state up to an instability point (section 2.4.7); in the OPP, steady oscillations are stablished the balance of the damping and the spin transfer torque.

The behavior of the angles inside TS can be understood in terms of the explanation given in section 2.4.7 for a structure that was easier to analyze: a perpendicular polarizer and an in-plane magnetic field. In that case, upon the injection of a current, the magnetization undergoes an in-plane rotation up to a certain angle when instability takes the magnetization to a dynamical state. In the case of the structure of this thesis, it is necessary to note two features about the TS region in figure 32. In the first place, the angle θ is determined primarily by the external field, it does not change with voltage. Secondly, φ does not vary with H_{app}, it is determined by the external voltage. Consequently, the difference with respect to the structure with an in-plane field, is that the starting point of the magnetization will not be in $\theta = \frac{\pi}{2}$, but with an angle that depends on the value and direction of H_{app}. Then, upon the application of a current the magnetization rotates just in φ, up to the moment when instability is reached and stationary oscillations are established, or, if H_{app} is too large another stable state will be attained, that corresponds to OPS.

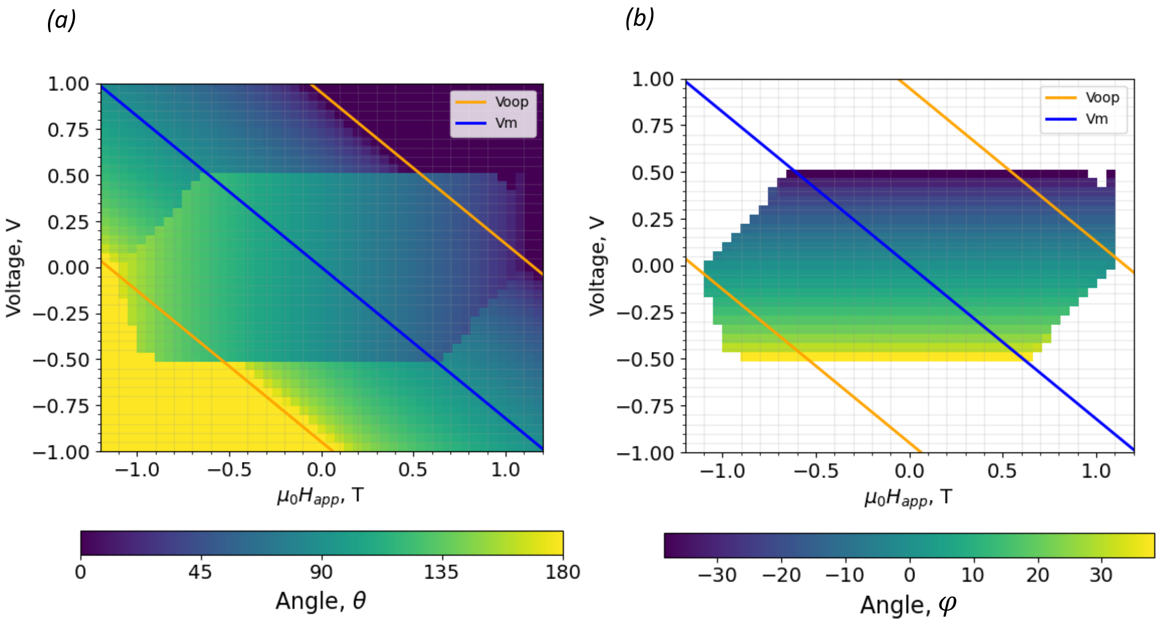

*Fig. 32. Angle θ and angle φ diagrams in (a) and (b) respectively. Free layer of 130x100 nm^2. Parameters M_s=1e6, K_u=0, α=0.01, **p**=(0,0,1). The applied field is out-of-plane.*

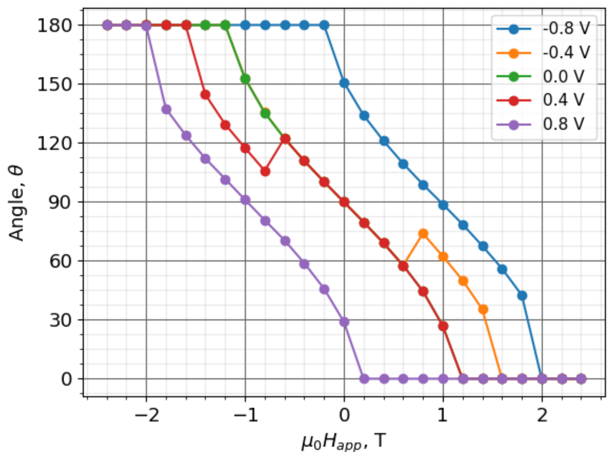

Fig. 33: Angle theta of the magnetization for different voltages and magnetic fields.

4.3. Effects of hysteresis

A hysteresis effect was already noted when discussing the voltage V_{stat}: the threshold voltage to transit from a static TS state to a dynamic OPP state or the converse is different when one takes into account the "history" of the magnetization. More simulations were performed to study the effect of hysteresis in the whole state diagram. They were performed for 0 K and 10 K and followed two schemes: the constant voltage one, that is based on sweeps throughout a range of magnetic field values for a constant applied voltage; the constant field one, which consists on sweeps throughout a range of voltage values for a constant H_{app}; moreover, the magnetization is never reset between simulation steps.

4.3.1. Voltage-Field state diagrams

For each one of the two simulation schemes mentioned previously, two different sweeps were made: a sweep up, where the starting point is the bottom left of the diagram, or in other words, the negative values of voltage and magnetic field, and the top right of the diagram is the end point; a sweep down, whose starting position is the top right of the diagram and it ends in the bottom left part of the graph.

First, the results of the constant voltage simulation scheme at 0 K are discussed. The diagrams obtained from these simulations, figure 34, have two features that are in contrast with respect to the case of no hysteresis: in the first place, for figures 34a and 34c, where the sweep up was made, the left boundary of OPP is shifted inside the region between the V_{oop} lines. Nonetheless, the right boundary of OPP is kept the same. Secondly, in figures 34b and 34d, where the sweep down was performed, the right boundary of OPP is displaced inside the area between the V_{oop} curves. However, the left boundary of OPP is kept the same. This means that there is a change in the threshold voltage needed to go from the OPS static regions to the OPP dynamic ones, but for the opposite transition this voltage is the same.

For 0 K one would expect that during the sweep through the OPS regions the magnetization reaches its maximum ($\theta = 0$ or equivalently m_z=1) and remains there, because once **M** is parallel to $\mathbf{H_{eff}}$ and **P** the torques are zero following the LLGS equation (eq. 5). However, what happens is that throughout the numerical calculations m_z approaches 1 in an asymptotic way as the time progresses. Thus, when the dynamic region is attained during the sweep, m_z is driven away from 1 slowly so that several simulation steps are required and as a consequence the already mentioned shift in the boundaries is present.

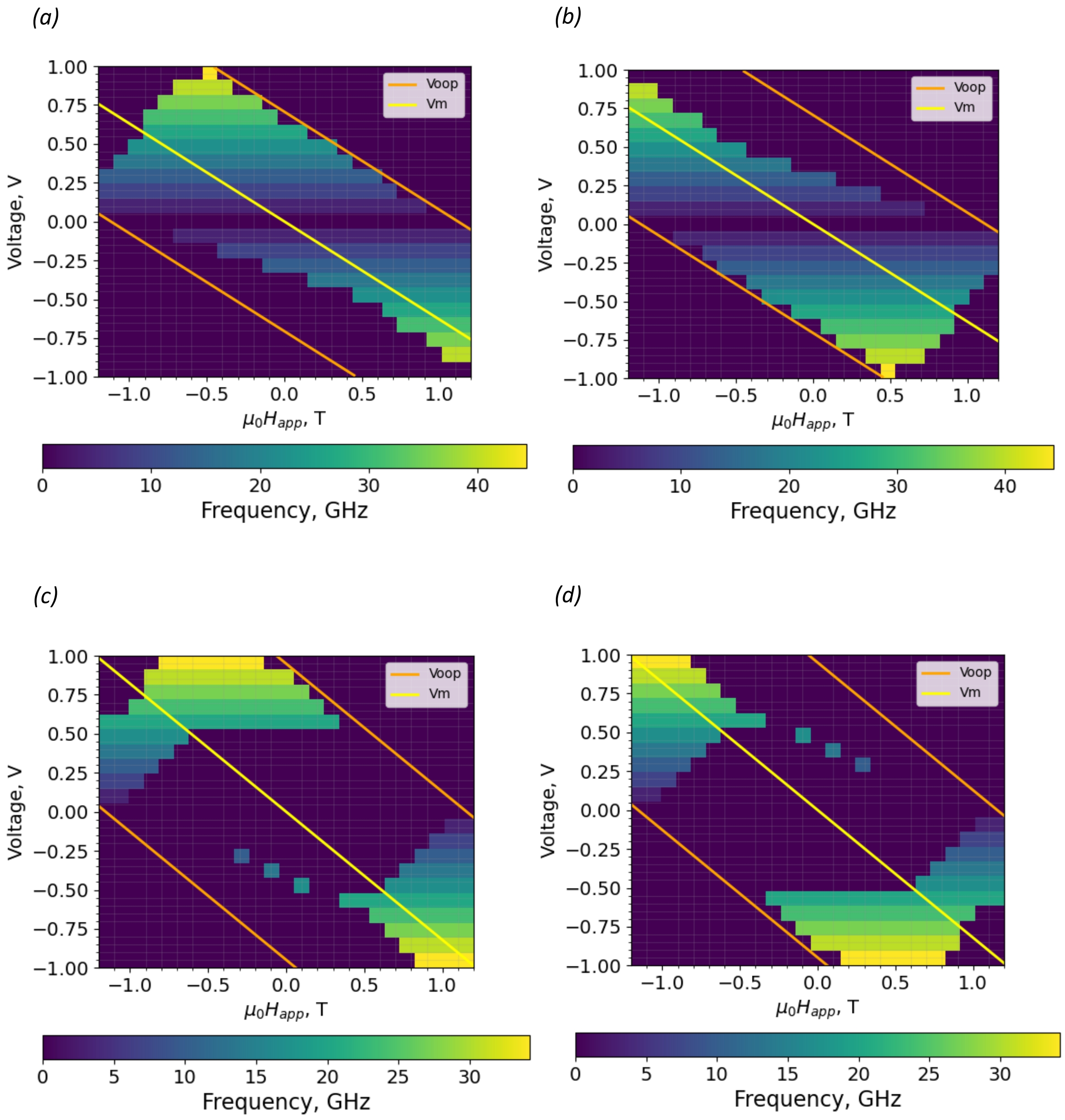

Fig. 34: Voltage field state diagrams obtained sweeping through the field for each voltage at 0 K. (a) and (b) are for the symmetric device, while (c) and (d) are for the asymmetric. In (a) and (c) a sweep up was performed and a sweep done for the case of (b) and (d).

A great difference with respect to figure 34 is observed when the temperature is increased to 10 K in the constant voltage simulation scheme: the shifts in the boundaries are not present any more, that is to say, the dynamic and static region follow the V_{oop} curve as figure 35 shows for the symmetric oscillator. What happens is that the stochastic thermal field perturbs the magnetization when it is in the OPS state, hence moving it away from the energy maximum and increasing the torques of the LLGS equation so that the OPP dynamic state is attained.

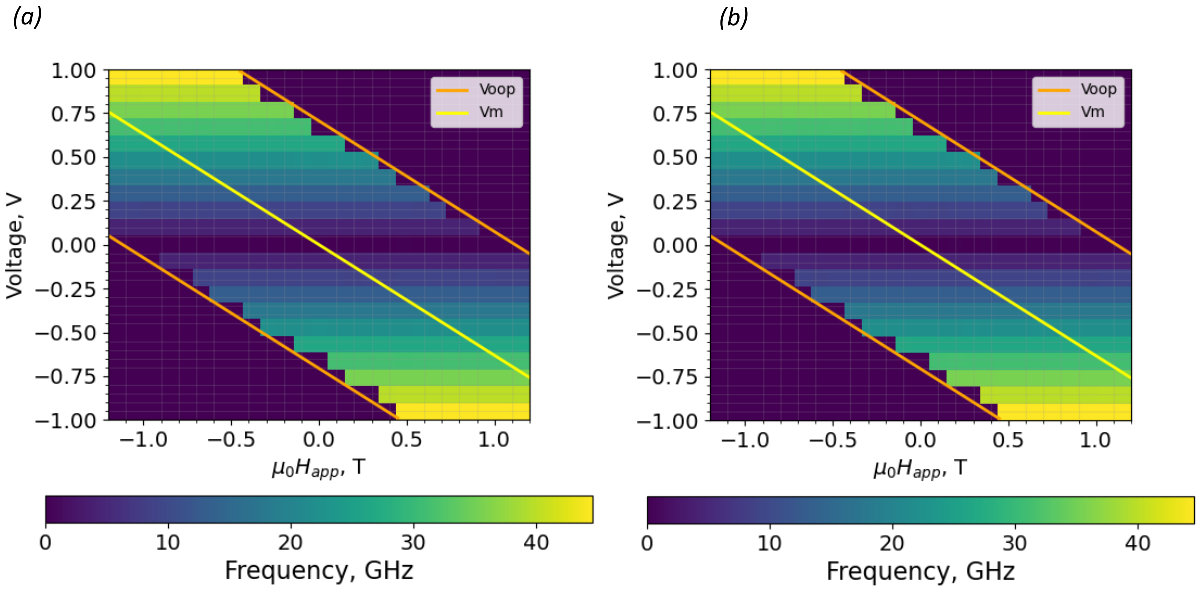

Fig. 35: Voltage field state diagrams of the circular device obtained sweeping through the field for each voltage at 10 K. For sweep up and down, (a) and (b) were obtained respectively.

Similar results are observed for the asymmetric device at 10 K, figure 36. Notwithstanding, there is a difference between the diagrams with no hysteresis at 0 K and 10K, that are depicted in figures 26b and 36c. In the second case, V_{stat} has a smaller value for a certain range of fields, approximately between -0.7 and -0.3 T for the positive V_{stat}. This may be due to transitions to OPP thanks to the energy provided by the thermal fluctuations.

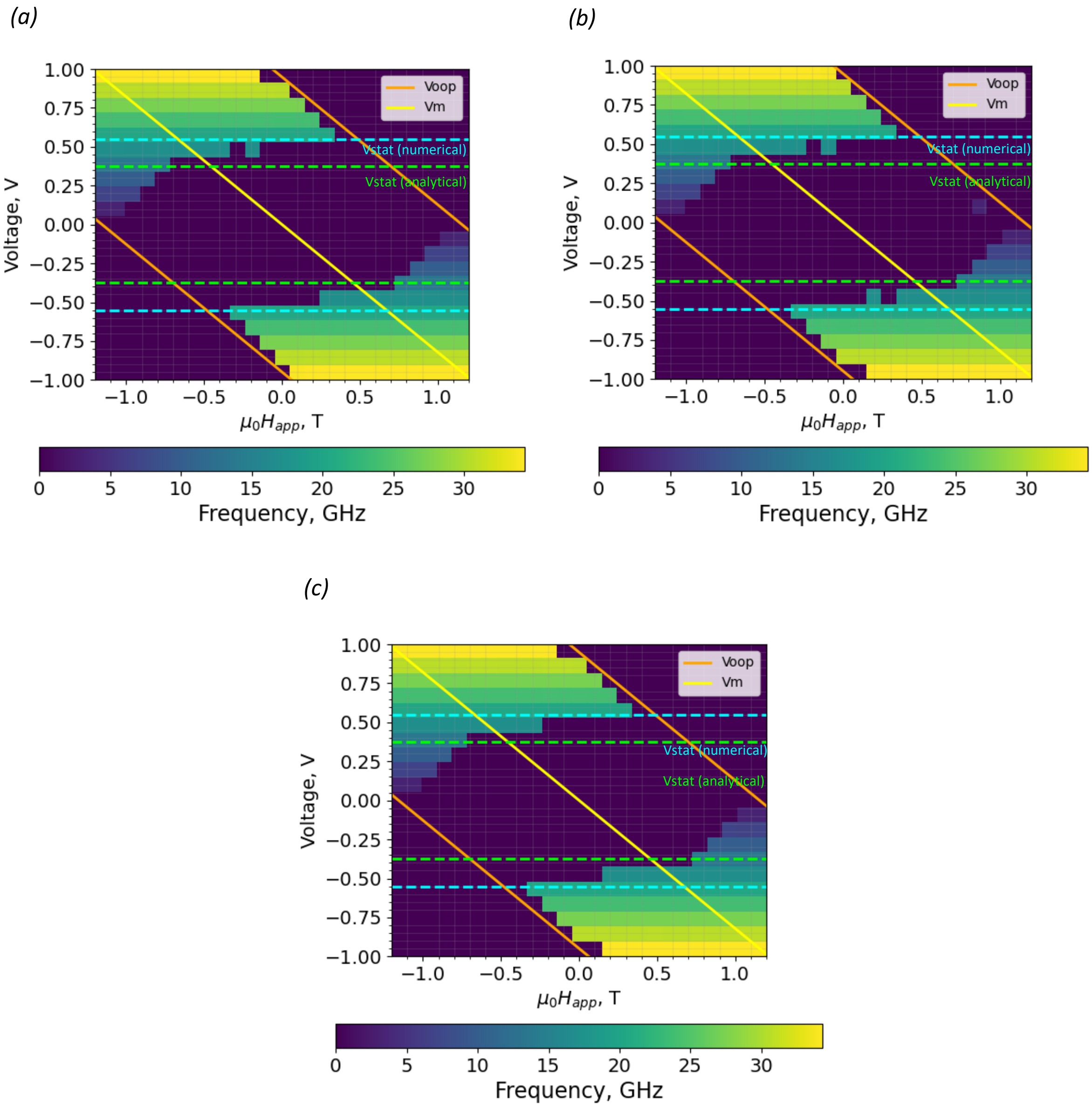

Fig. 36: Voltage field state diagrams of the elliptical device obtained sweeping through the field for each voltage at 10 K. The results from sweep up and down are (a) and (b) respectively. (c) shows the voltage-field diagram without hysteresis at 10 K.

In the case of the constant field simulation scheme at 10 K, the results for the symmetric device show no shift of the boundaries as in the instance of figure 35. Secondly, for the asymmetric device (figure 37) there is an evident discrepancy in the value of the V_{stat} with respect to the numerical one from figure 26b. This effect still has to be understood.

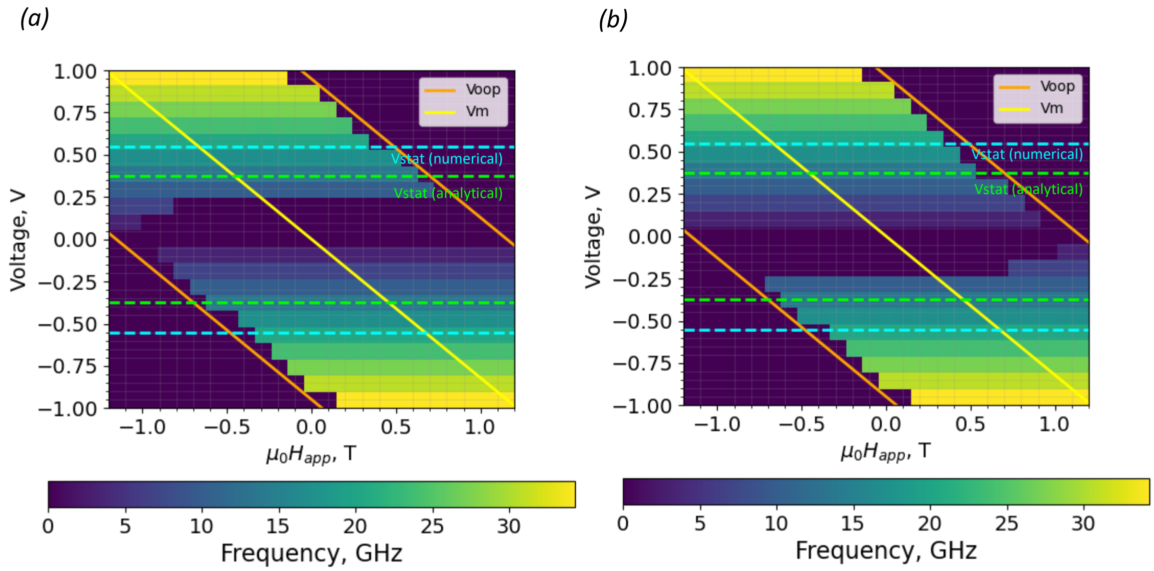

Fig. 37: Voltage field state diagrams of the elliptical device obtained sweeping through the voltage for each magnetic field value at 10 K. The results from sweep up and down are (a) and (b) respectively.

5. Injection locking results

So far, the dynamics of a single oscillator have been analyzed under different conditions, but as mentioned before, other phenomena like synchronization to an external signal or other oscillators are of interest.

Some definitions have to be made before presenting the results. In the first place, a STNO can be classified within the class of **auto-oscillator.** This is an oscillator that meets three requirements [12]:

(i) It has an internal source of energy that compensate losses, thus, even if isolated it continues oscillating. In an STNO this energy source is given by the injected current.
(ii) It is stable with respect to perturbations. In fact, a limit cycle, a stationary oscillatory state mentioned in section 2.4.7, is characterized by the stability of its trajectory. This means that if the amplitude of oscillations is perturbed some external factor, the system will recover the original amplitude value.
(iii) The shape of the oscillations is determined by the parameters of the system, not by how it is switched on, or in other words, the oscillation amplitude of a limit cycle does not depend on initial conditions. In a STNO for example the condition for precession is given by the critical current that depends on parameters like the thickness of the free layer, the saturation magnetization, the polarization efficiency and the different contributions to the effective field.

In the second place, the concept of **synchronization** can be understood as the adjustment of the oscillatory motion of two auto-oscillators through a weak coupling that results in **frequency locking**, because the frequencies become the same, and a constant phase relationship, that is called **phase locking**. Therefore, if two oscillators are considered, they have frequencies f_1 and f_2 when isolated, which can be called *natural* frequencies following [12]; but when coupled they oscillate with a common frequency.

Synchronization depends on two factors:

- **Coupling strength:** it refers to how weak or strong the interaction is.
- **Frequency detuning:** it is a measure of how different the uncoupled auto-oscillators are. Its value is $\Delta f = f_1 - f_2$. Furthermore, the range of detuning in which the oscillators can still couple is called **phase locking bandwidth**.

When an auto-oscillator is isolated, its phase does not have a preferred value i.e. its phase is free while the amplitude has a well defined value (given by the balance of positive and negative dissipation). Hence, after a perturbation, the phase will not go back to a certain equilibrium value, the perturbation will persist because of the marginal stability of the phase. This sensitivity to an external influence is what makes synchronization possible, this allows the oscillator to couple with an external signal.

In this and the following section two cases will be addressed: the first one is **injection locking**, where the STNO is coupled to a RF signal that is added to the injected current. In this case, it is expected that under synchronization the oscillator's frequency (f_{STO}) follows the external RF frequency (f_{RF}). The second case consists of two STNOs that couple through the interaction due to the **dipolar field**.

The **simulation scheme** for injection locking was the following: A certain DC voltage is applied as usual*, and* after some nanoseconds the RF signal is imposed, figure 38. The phase locking bandwidth was evaluated sweeping the RF frequency and checking if the STNOs frequency follows it. In this context, two different types of injection locking will be considered depending on the value of the RF frequency with respect to the natural frequency of the oscillator: *f locking* means that f_{RF} is swept around f_{STO}, while *2f locking* alludes to the case when f_{RF} is swept around $2f_{STO}$ when it exists.

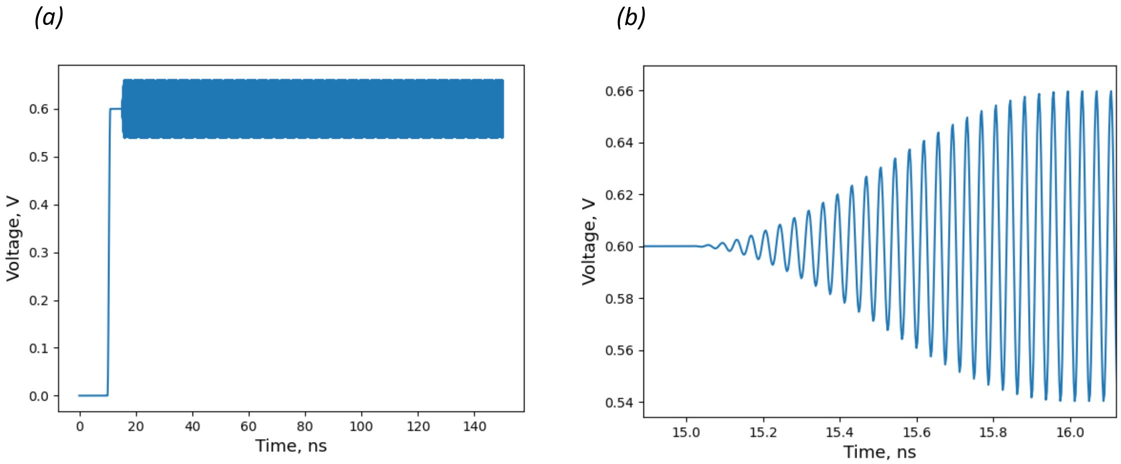

Fig. 38. Input voltage for injection locking. (a) Voltage step applied through all the simulation time. First a DC value is imposed and after some nanoseconds a sinusoidal signal is added. (b) Voltage applied. The AC signal is applied gradually and has an amplitude of 0.06 V.

5.1 Symmetric device

5.1.1. OPP mode (using OP polarizer)

We have chosen operational conditions for the simulations, where the natural frequency of the STNO is 26.65 GHz, which corresponds to the case when a voltage of 0.6 V is applied. The RF signal is swept between 26.63 and 26.67 GHz as figure 39 indicates, but the phase locking bandwidth is zero.

Since the sweep is performed with a step of 10 MHz, a longer time trace was generated so that the resolution of the frequency given by the FFT is 3.3 MHz.

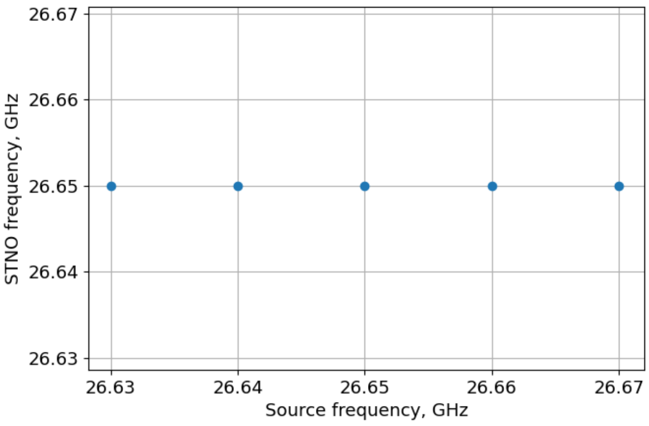

Fig. 39. STNO frequency vs RF frequency. Free layer of 100x100x3 nm. Parameters M_s= 1e6 A/m, K_u= 0 J/m^3, α=0.01, p = (0,0,1). H_{app}= -0.1 T. DC voltage = 0.6 V.

5.1.2. IPP mode (using IP polarizer)

For the evaluation of synchronization with an IPP mode, magnetocrystalline anisotropy was added to the structure. *f* and *2f* locking were verified (figure 40), and the results indicate that the phase locking bandwidth for the sweep around $2f_{STO}$ is of 400 MHz.

For *f* locking, the resolution of the FFT is of 3.3 MHz. Besides, for the *2f* case, since the phase locking bandwidth is of several hundreds of MHz, the resolution of the FFT is 10 MHz.

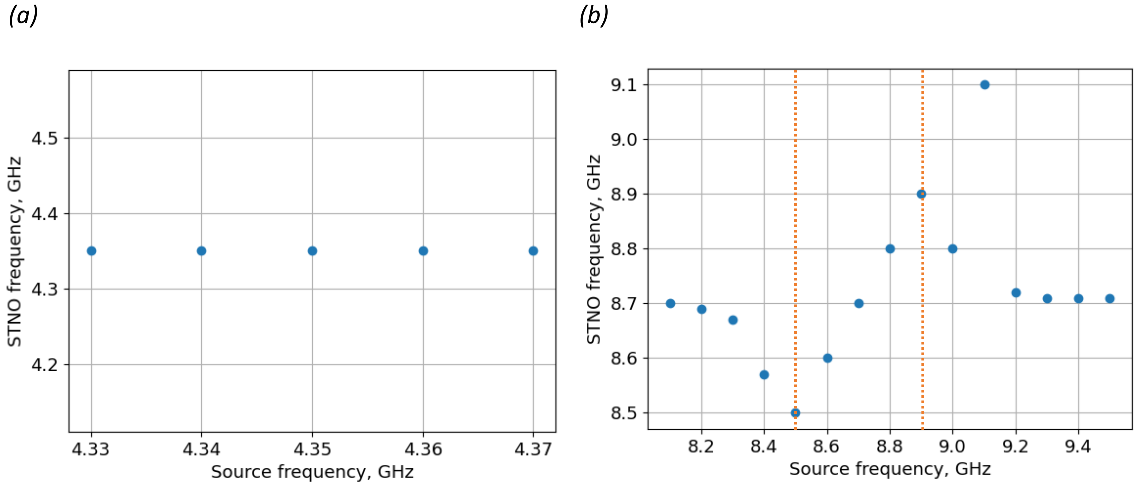

Fig. 40: STNO frequency vs RF frequency. Free layer of 100x100x3 nm. Parameters M_s= 1e6 A/m, K_u = 1e4 J/m^3, α= 0.01, p=(0,0,1). H_{app}= 0.03 T. DC voltage = 0.5 V. (a) RF frequency sweep around f. (b) RF frequency sweep around 2f; the phase locking bandwidth is indicated by the orange dashed lines.

5.2. Asymmetric device

5.2.1. OPP mode (using OP polarizer)

The asymmetric STNO has two frequency components, as discussed in section 3.4.3. The voltage imposed to the device is 0.6 V, that leads to frequencies f_{STO}=20.50 GHz and $2f_{STO}$=41 GHz. The results of the simulations with the RF signal are depicted in figure 41. For 2f locking, that is, around 41 GHz, the phase locking bandwidth is 30 MHz.

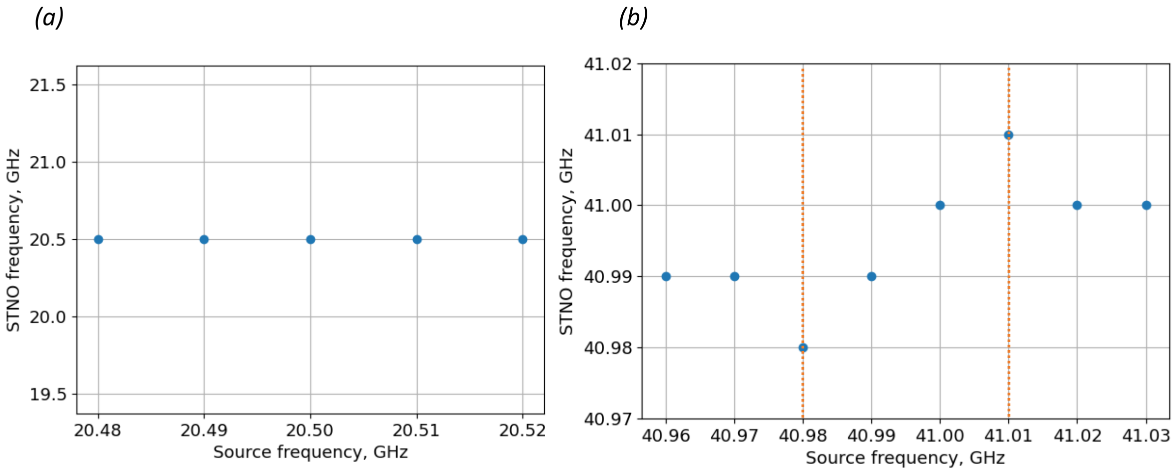

Fig. 41: STNO frequency vs RF frequency. Free layer of 130x100x3 nm. Parameters M_s*= 1e6 A/m,* K *= 0 J/*m^3*, α= 0.01, p = (0,0,1).* H_{app}*= -0.1 T. DC voltage = 0.6 V. (a) RF frequency sweep around f. (b) RF frequency sweep around 2f; the phase locking bandwidth is indicated by the orange dashed lines.*

5.3. Effect of hysteresis

The effect of hysteresis was checked by not resetting the magnetization during the frequency sweeps. In each case, a sweep up was made from f_{STO} or $2f_{STO}$ to larger frequencies, and a sweep down from f_{STO} or $2f_{STO}$ towards smaller frequencies.

For the device with the IPP mode, the phase locking bandwidth is increased from 400 to 700 MHz, as can be noted from figure 42. On further consideration, this bandwidth decreases from 30 to 10 MHz in the asymmetric device. Table 6 summarizes the results of this section.

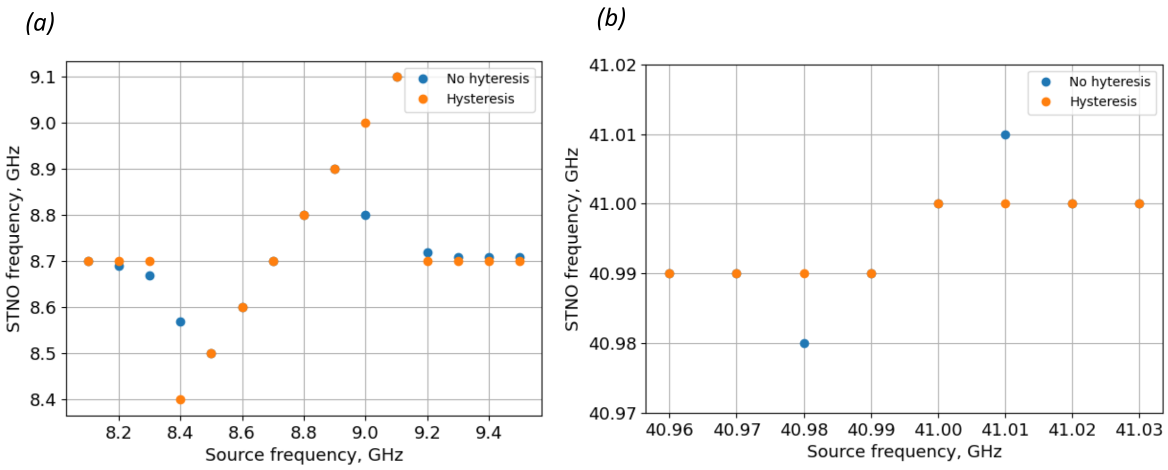

Fig. 42: STNO frequency vs RF frequency. The results with and without hysteresis effects are compared. (a) shows the results for the device with the IPP mode. (b) depicts the outcome with the asymmetric device. Both cases correspond to 2f locking.

Type of STNO	**Mode**	**Injection locking**	**Phase locking bandwidth, MHz**	**Phase locking Bandwidth (hysteresis), GHz**
Symmetric	OPP, f	No	0	0
	IPP, f	No	0	0
	IPP, 2f	Yes	400	700
Asymmetric	OPP, f	No	0	0
	OPP, 2f	Yes	30	10

Table 6.

6. Two STNOs synchronization, results

In this section, the analysis is on two symmetric STNO, that interact thanks to their dipolar fields. Various situations are presented for the symmetric device, for which the external parameters are varied in different ways and two separation distances between the oscillators are considered.

Eq. 21 is the expression of the dipolar field acting on the device *i* due to the oscillator *j. V* is the volume, r_{ij} is the vector going spatially from *j* to *i,* and *dx, dy* and *dz* are the components of this vector.

$$Hc_{xi} = \frac{M_{sj}V_j}{4\pi}\left[\frac{(\boldsymbol{m_j}\cdot\boldsymbol{r_{ij}})dx_i}{|\boldsymbol{r_{ij}}|^5} - \frac{m_{xj}}{|\boldsymbol{r_{ij}}|^3}\right] \quad (21a)$$

$$Hc_{yi} = \frac{M_{sj}V_j}{4\pi}\left[\frac{(\boldsymbol{m_j}\cdot\boldsymbol{r_{ij}})dy_i}{|\boldsymbol{r_{ij}}|^5} - \frac{m_{yj}}{|\boldsymbol{r_{ij}}|^3}\right] \quad (21b)$$

$$Hc_{zi} = \frac{M_{sj}V_j}{4\pi}\left[\frac{(\boldsymbol{m_j}\cdot\boldsymbol{r_{ij}})dz_i}{|\boldsymbol{r_{ij}}|^5} - \frac{m_{zj}}{|\boldsymbol{r_{ij}}|^3}\right] \quad (21c)$$

6.1. Identical STNO and identical external parameters

In this case, the external parameters of both STNOs, that is, the external field H_{app} and the voltage, are the same.

In the first place, the dynamics for 30 nm of separation between the STNOs are analyzed. From the results, figure 43, it can be noted that the major difference from the isolated oscillator in figure 16 is the presence of a gap, similar to the TS region in the asymmetric device. This effect resembles shape anisotropy, as if the isolated device had changed its dimensions (the two STOs see each other through the dipolar interaction, since they are identical and oscillate at the same frequency, they see each other dipolar field, and this results in an effective dynamic shape anisotropy). Nevertheless, the behavior of the frequency and the angle θ with respect to the voltage and field is the same as the individual oscillator.

According to figure 44 the phase difference between the two STNOs is defined just for the dynamic OPP region in figure 43 and it is equal to zero. Moreover, figure 44 shows that considering both the isolated and the present Voltage-Field diagrams, the only difference is the already mentioned gap. Outside it, the frequencies for each voltage and external field are the same, except from two yellow points that are simulation artifacts.

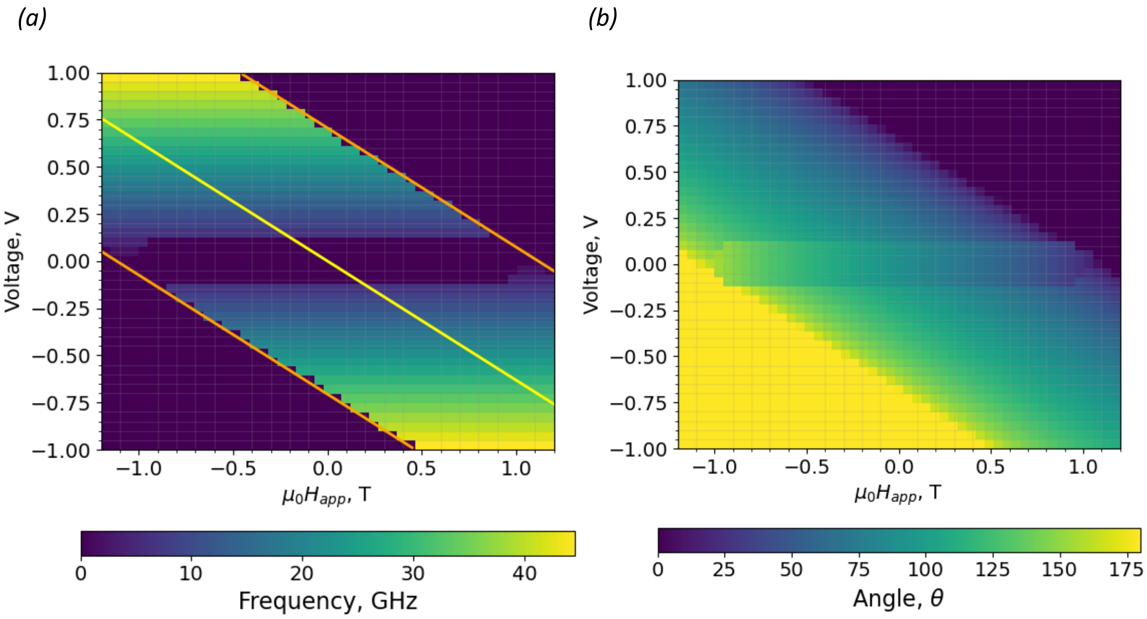

Fig. 43: Voltage-Field state diagram (a) and angle θ diagram (b). Free layer of 100x100x3 nm. 30 nm of separation. Parameters M_s= 1e6 A/m, K_u= 0 J/m^3, α=0.01, p = (0,0,1).

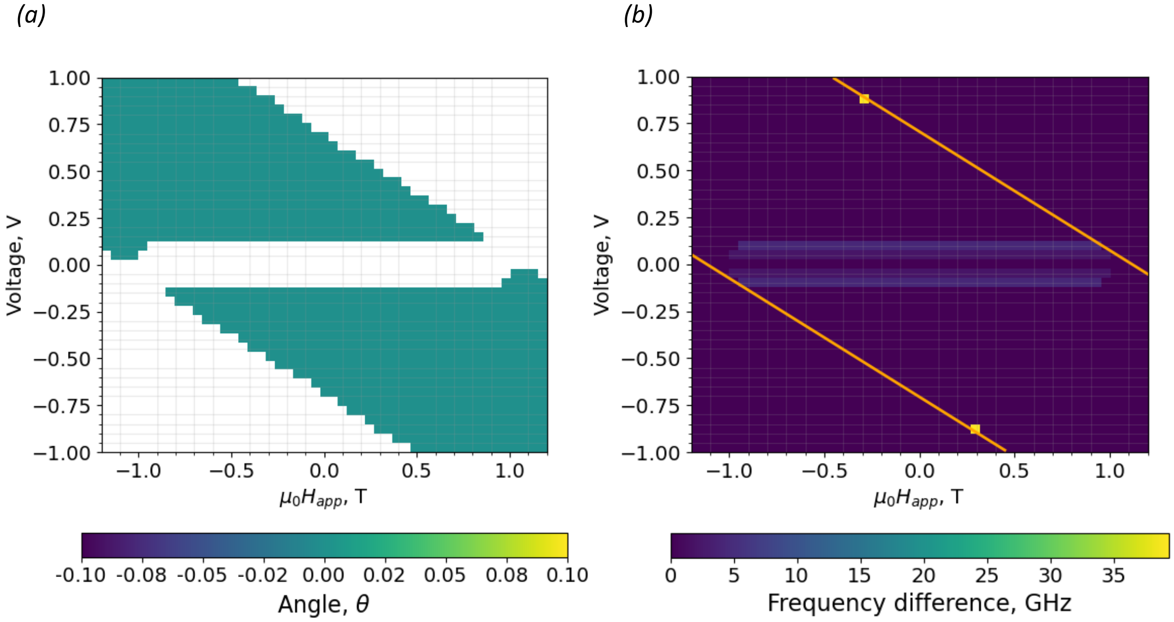

Fig. 44: The diagram in (a) shows the phase difference between the two STNOs. In (b) the difference of the Voltage-Field diagram with respect to the isolated oscillator is depicted. Free layer of 100x100x3 nm. 30 nm of separation. Parameters M_s= 1e6 A/m, K_u= 0 J/m^3, α=0.01, p = (0,0,1).

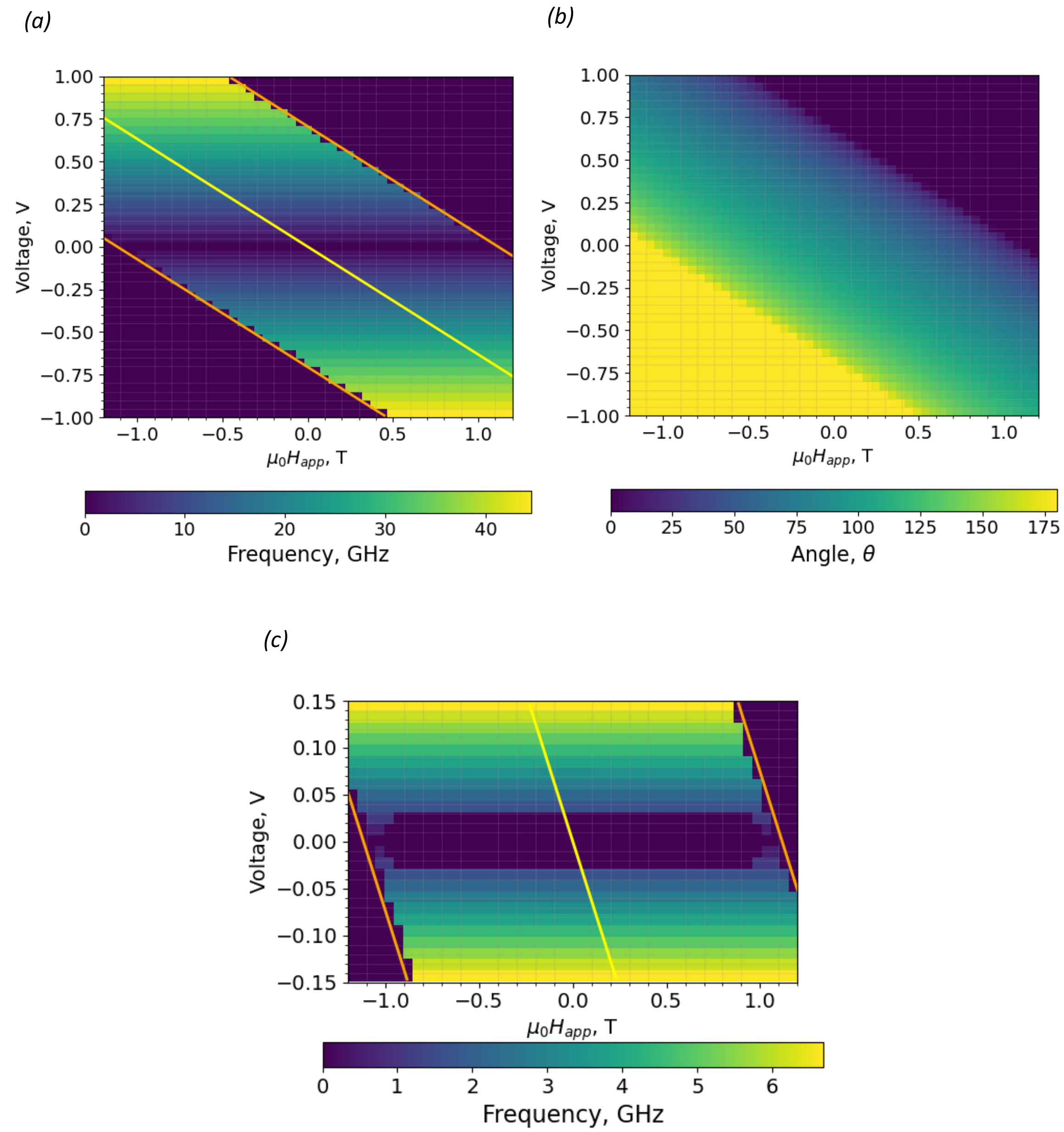

Fig. 45: Voltage-Field state diagram (a), angle θ diagram (b) and Voltage-Field state diagram with a finer step (c). Free layer of 100x100x3 nm. 100 nm of separation. Parameters M_s= 1e6 A/m, K_u= 0 J/m^3, α=0.01, p = (0,0,1). Thetat diagram for (c)?

The phase difference, as can be noted from figure 46a has the same behavior as the previous case. In the second place, the frequencies for each voltage and field are still the same with the exception of the area of the gap.

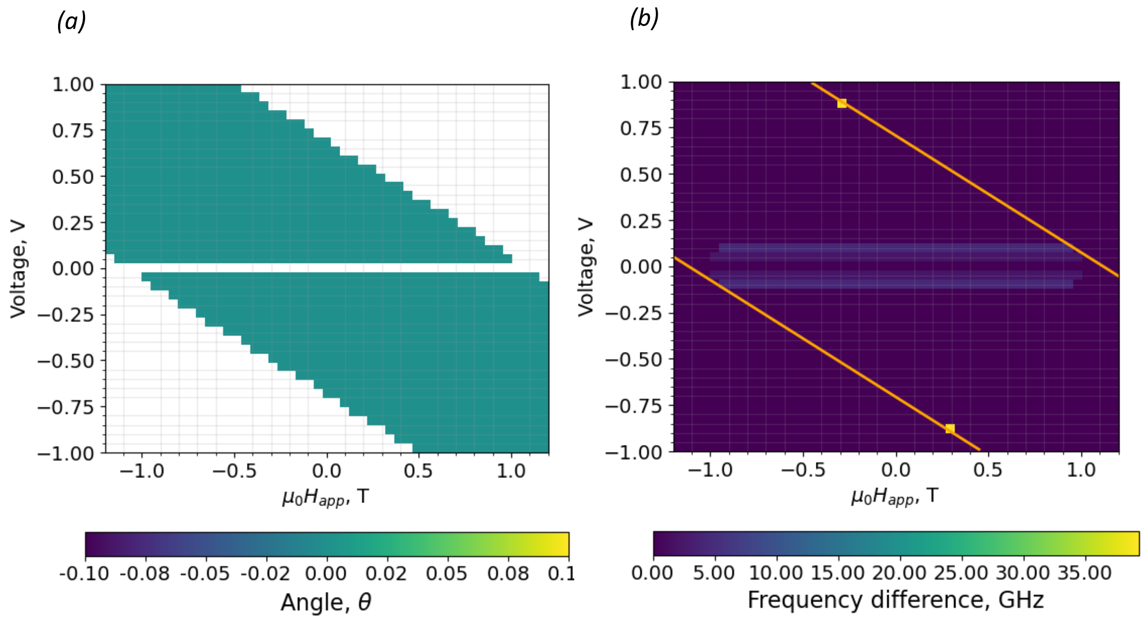

Fig. 46: The diagram in (a) shows the phase difference between the two STNOs. In (b) the difference of the Voltage-Field diagram with respect to the isolated oscillator is depicted. Free layer of 100x100x3 nm. 100 nm of separation. Parameters M_s= 1e6 A/m, K_u= 0 J/m^3, α=0.01, p = (0,0,1).

6.2. Non-identical external parameters: V of one STNO fixed

For the analysis in this section, the simulations followed this approach: at a certain common magnetic field, the voltage of one STNO was kept constant at 0.4 V while the other is swept within a voltage range, between 1 and -1 V; the temperature is 10 K. The results are used to study how the phase locking bandwidth, the 3D trajectories and the symmetry of the synchronization are affected by parameters like the separation between the devices and the magnetic field.

For the discussion and figures, the voltage varying STNO is the number 1, and the fixed voltage STNO is the number 2.

6.2.1 Separation of 100 nm

In the first place, the case of 100 nm of separation is studied for four different values of magnetic field: 0, -0.35, -0.40, -0.45 T. The results corresponding to the first value are presented in figure 47, where subfigures c and d show the sweep around -0.4 and 0.4 V with a finer step. In the first place the phase locking bandwidth is not large enough to be evident with an step of 0.05 V; secondly, the finer sweeps reveal that the synchronization range is higher for the negative voltage, which is due to the fact that the anti-parallel orientation of the magnetization of the two devices minimizes the energy with respect to a parallel configurations.

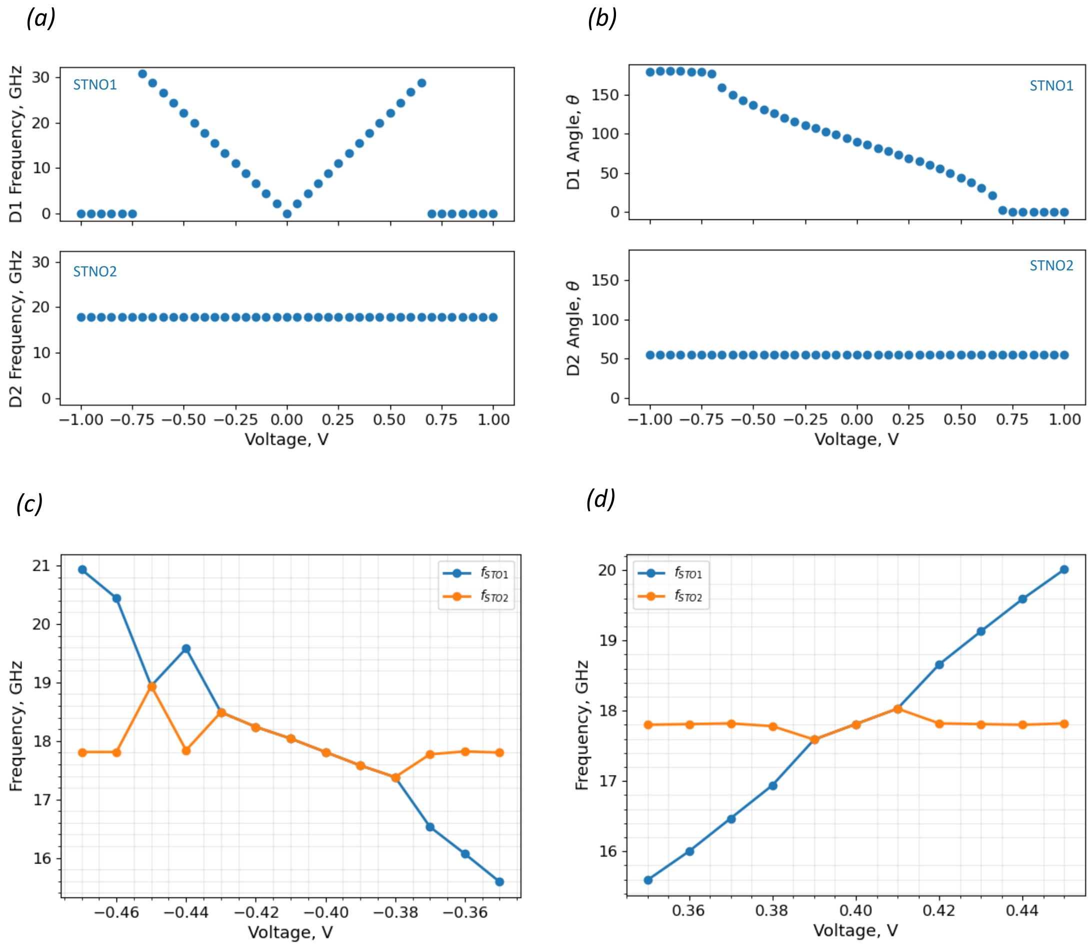

Fig. 47: Results for two STNOs separated by 100 nm. $\mu_0 H_{app}$=0 T. (a) Frequency vs Voltage. (b) angle θ vs Voltage. (c) and (d) are sweeps with a finer voltage step around -0.4 and 0.4 V respectively .

The results for the other mentioned magnetic fields, depicted in figure 48, give the impression that the phase locking bandwidth is several times larger than the previous instance of figure 47. Nevertheless, recalling the first feature of auto-oscillators mentioned at the beginning of section 5, these oscillators must be able to oscillate if isolated. Thus, for voltages larger than V_{oop} the STNO1 does not behave as an auto-oscillator, and if it still follows the STNO2, their interaction cannot be called synchronization anymore. In figure 48 this observation is valid for voltages at the left of the dashed lines, that indicate V_{oop}.

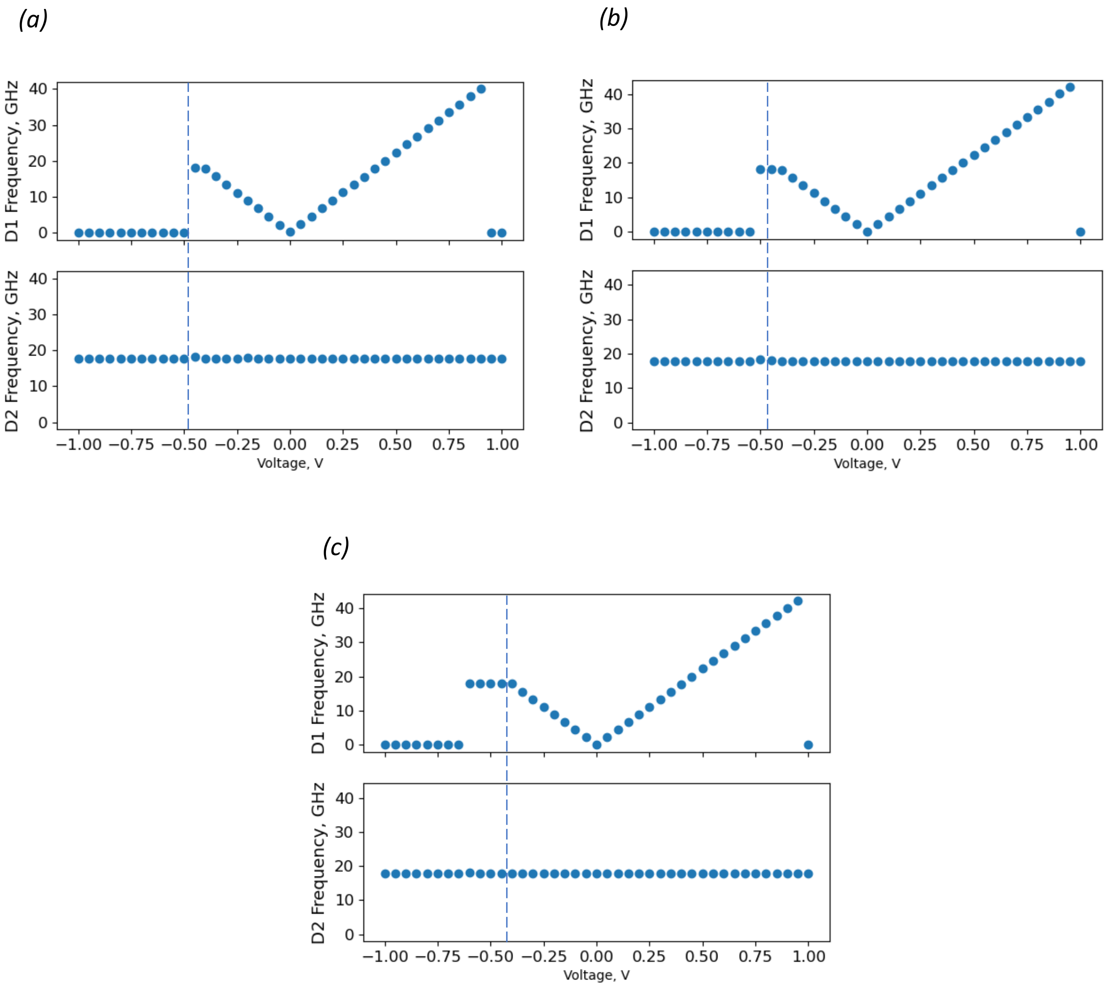

Fig. 48: Frequency vs Voltage plots for two STNOs separated by 100 nm. The dashed lines indicate V_{oop}. (a) $\mu_0 H_{app}$=-0.35 T. (b) $\mu_0 H_{app}$=-0.40 T. (c) $\mu_0 H_{app}$=-0.45 T.

When two oscillators are identical, the influence they exert on each other is the same and hence when they reach a common frequency under synchronization, it will be $\frac{f_1+f_2}{2}$. In the present situation, the strength of the effect that one oscillator has on the other is given by the oscillation amplitude.

For the case in figure 48a, some synchronization points are plotted in figure 49a. It is easy to note that the synchronization is symmetric, because as it is noted in figure 49a, the frequency f_{STO1} changed more than f_{STO2} when synchronization started. This “asymmetry” in the coupling is due to the fact that the oscillators have different amplitudes and hence produce different dipolar fields as figures 49a to d demonstrate. Hence, how mutual is the synchronization can be varied through the external magnetic field that changes the amplitude of oscillation.

Moreover, in order to minimize the dipolar energy, the magnetization of STNO2 rotates in the opposite sense of STNO1 as figure 49b denotes.

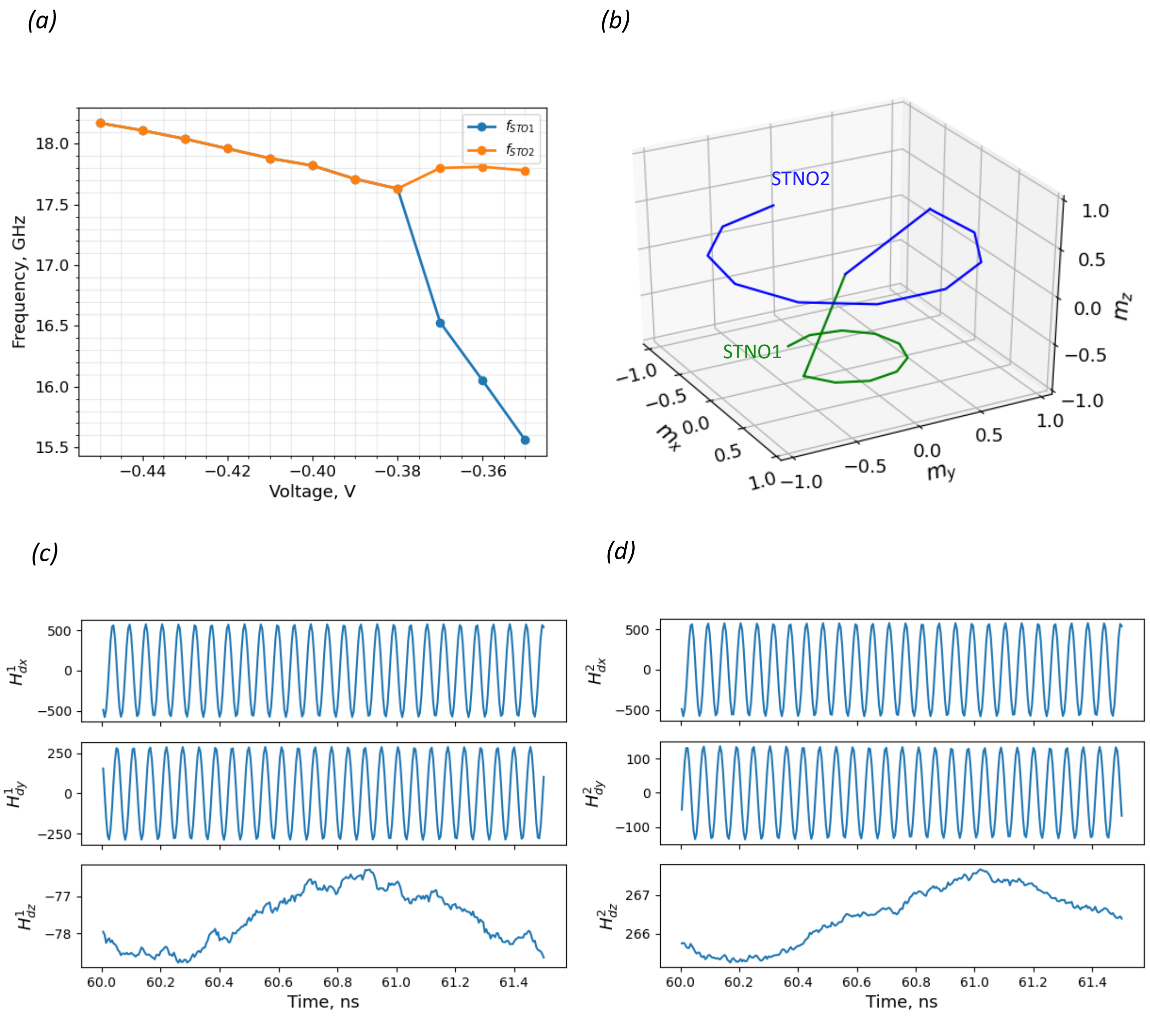

Fig. 49: Some features of two STNOs separated by 100 nm, at -0.35 T. STNO1 voltage: -0.4 V (a) some synchronization points. (b)Trajectories of the two STNO that denote the direction of oscillation and their amplitudes. (c) Dipolar field H_c seen by STNO1 (d) H_c seen by STNO2.

Increasing the coupling strength causes the phase-locking bandwidth to become larger. This is demonstrated in figure 50, where STNO frequencies are plotted for different external magnetic fields, that imply different amplitudes and coupling strengths. Within the range considered, as the external magnetic field becomes more negative, the amplitude of STNO2 increases and then the phase locking bandwidth grows, as it is more clearly represented by figure 50d, which is the so called *Arnold Tongue*.

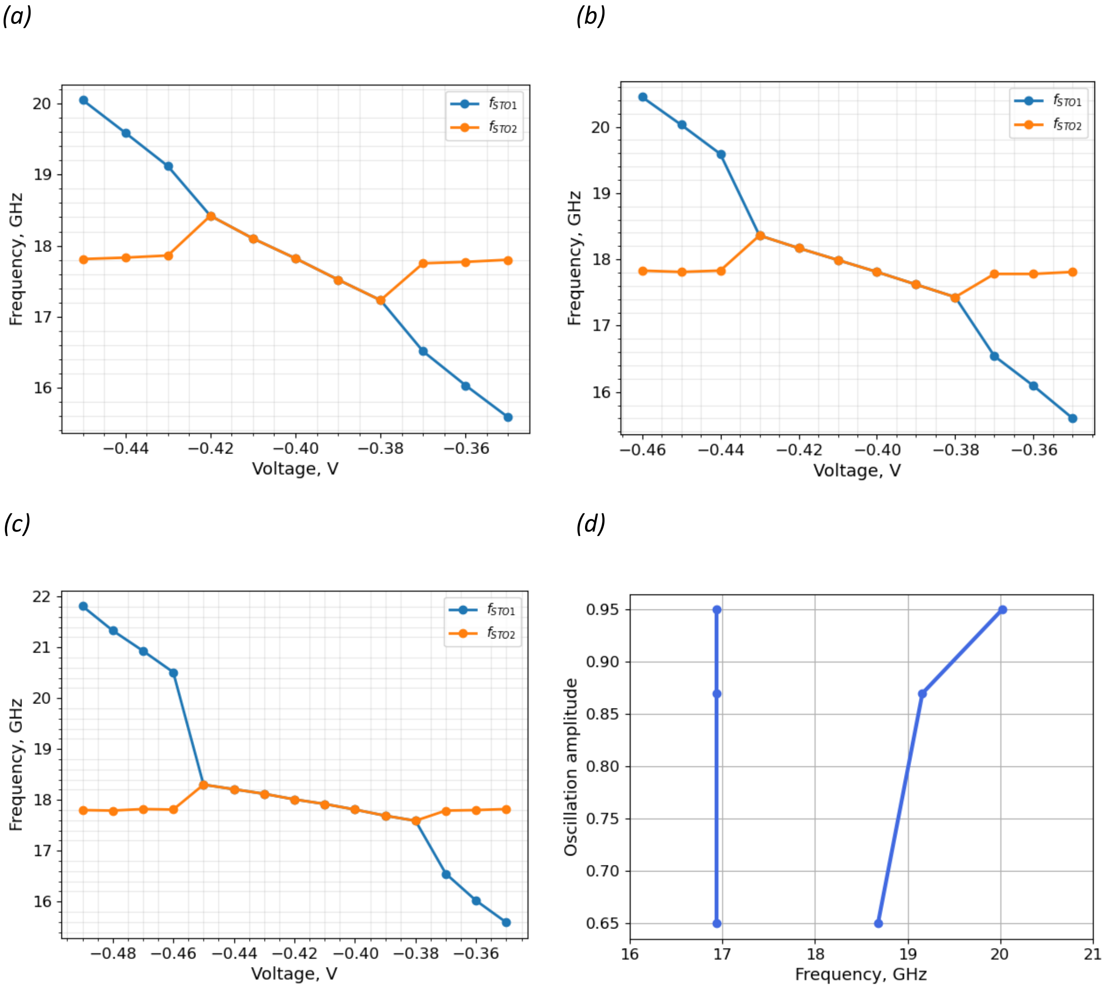

Fig. 50: Two STNOs separated by 100 nm. (a) $\mu_0 H_{app}$=0.2 T. (b) $\mu_0 H_{app}$=-0.1 T. (c) $\mu_0 H_{app}$=-0.3 T. (d) Arnold Tongue for which the separation between the two blue curves at each point is the phase locking bandwidth at a certain field.

6.2.2 Separation of 30 nm

For the case of 30 nm of separation between the two STNOs the phase locking bandwidth is compared with the previous case of 100 nm separation.

According to the results for an external field of 0 T, figure 51, the phase locking bandwidth is increased with respect to figure 47. This is explained by the fact that at a smaller distance, the coupling strength is larger, because the dipolar or stray field is strongly dependent on the distance as eq. 21 shows.

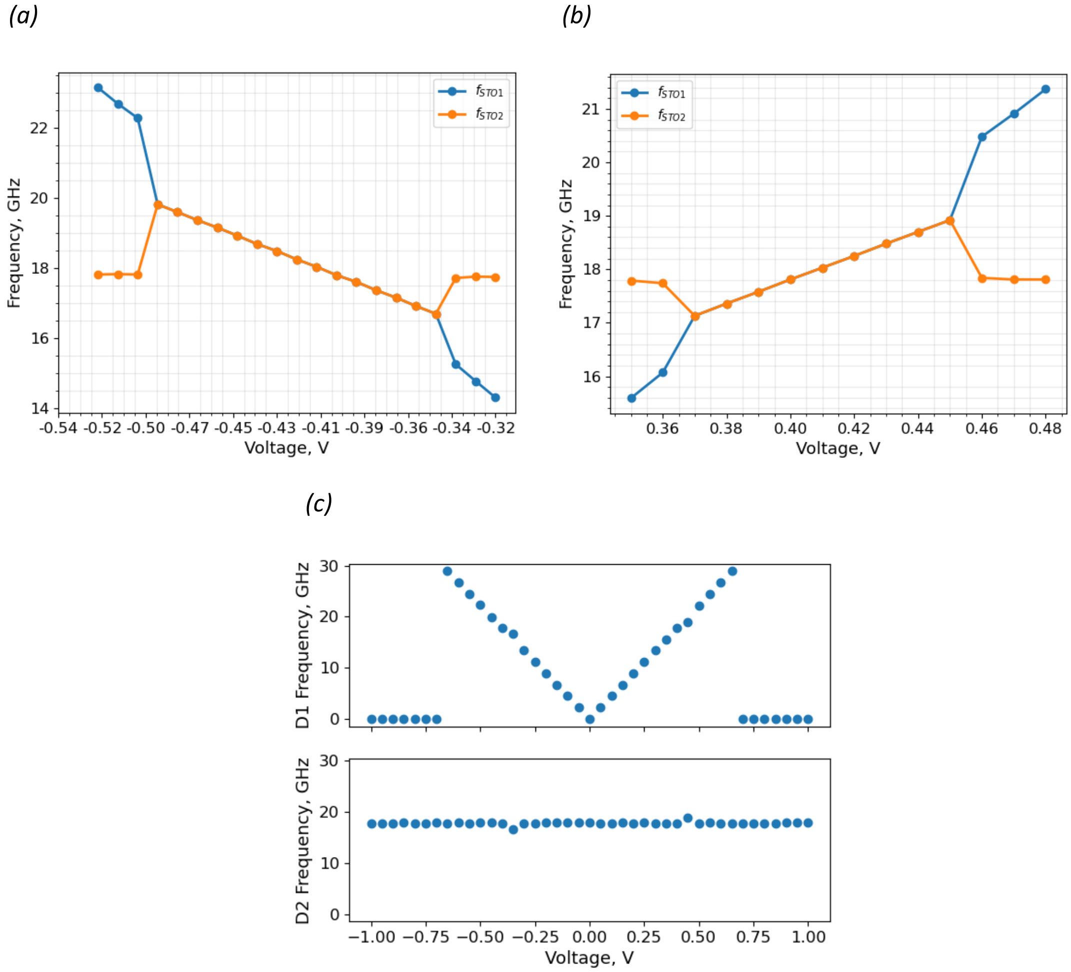

Fig. 51: Frequency vs Voltage for two STNOs separated by 30 nm. $\mu_0 H_{app}$=0 T. (a) and (b) are sweeps with a finer voltage step compared to (c)

At 0 T, when the voltage of both oscillators is the same (0.4 V), their synchronization is mutual, because their amplitudes of oscillation are equal (figure 52c). Thus, the dipolar field each oscillator sees is of the same order of magnitude (figure 52a and b).

When the magnetization of the two devices is oriented in the same out of plane direction, it rotates in the same direction to minimize dipolar energy (figure 52c).

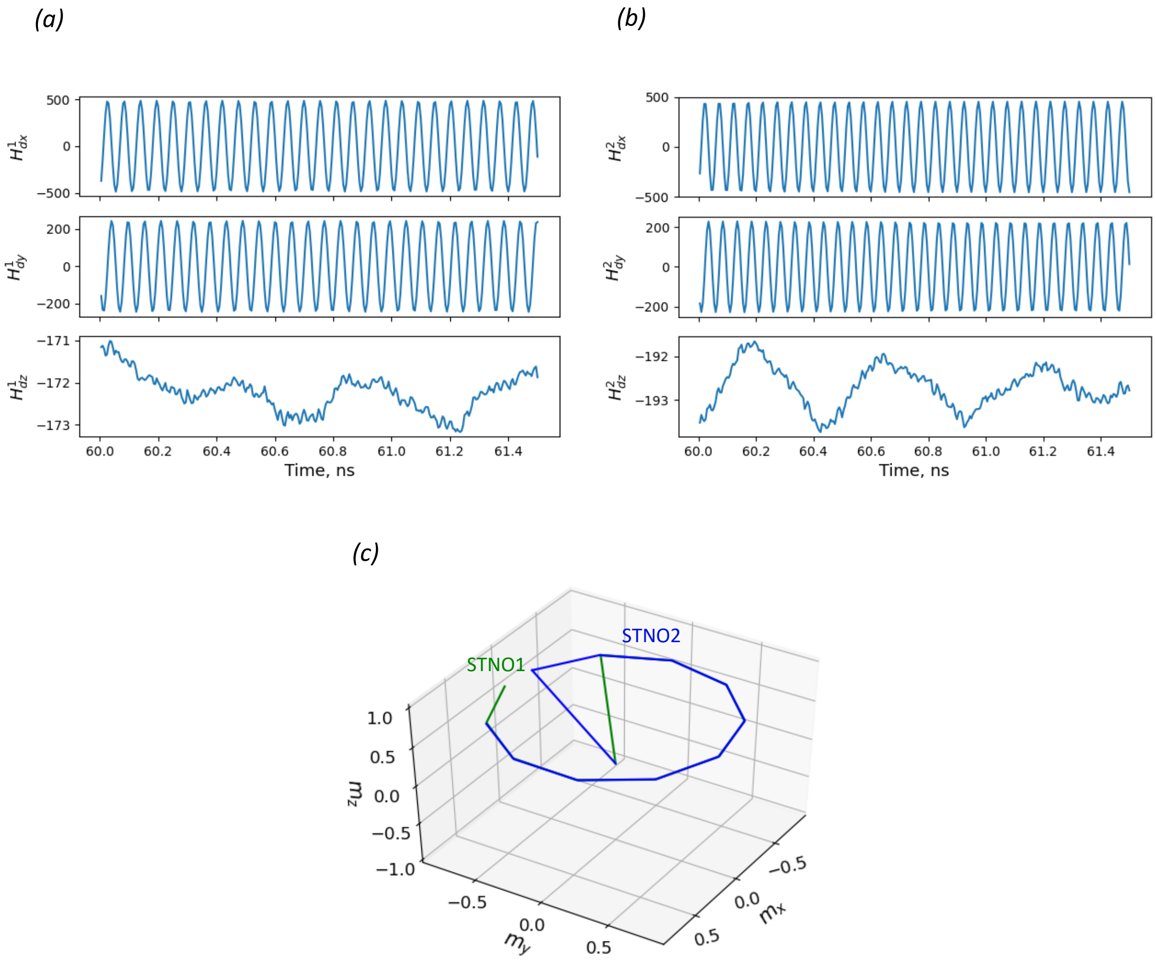

Fig. 52: Results for two STNOs separated by 30 nm. $\mu_0 H_{app}$=0 T and V = 0.4 V. (a) and (b) are the dipolar fields seen by STNO1 and 2 respectively. (c) shows the trajectories of the two STNO that denote the direction of oscillation and their amplitudes.

7. Conclusions and perspectives

In this work we have undertaken a simulation study of Spin Torque Nano-Oscillators (STNO), to understand the physics of a single one and the synchronization of it through Injection Locking with an external RF signal or dipolar interaction with another oscillator. These spintronic devices have an interesting feature that is the possibility of controlling the frequency changing the amplitude of oscillations. Besides, they offer potential applications in communications and Machine Learning. The specific structure considered in this thesis is based on a Magnetic Tunnel Junction (MTJ), a perpendicular polarizer and an out of plane magnetic field.

The analysis of STNOs is a complex task because it involves understanding of concepts of solid-state physics and more specifically of spintronics and magnetization dynamics as well as synchronization and non-linear dynamics properties. Furthermore, even when a single of these devices is considered, there are several parameters that affect its performance, it may operate in different dynamic regions and its state may depend on its history (hysteresis).

The large amount of data that results from simulations requires a careful treatment of it, which involves the proper documentation of all the parameters used during the numerical computations.

The STNO structure considered in this work exhibits an unexpected frequency dependence on magnetic field and voltage that may be useful for applications; for a certain voltage, this frequency can be kept constant while the magnetic field changes and modify the oscillations amplitude.

A change in dimensions, symmetry, or the presence of coupling between two STNOs can change the boundaries in the voltage-field state diagram of a single device, expanding or squeezing the different dynamic regions. More specifically, the TS region is enlarged when shape anisotropy is present in the structure or if there is coupling through the dipolar field with another oscillator, moreover a different area of the device affects the boundaries of the OPP zone and the frequency at each point.

Hysteresis was found to have an influence on the extension of the TS region in the voltage-field state diagram of a single oscillator, and on injection locking with a RF external signal.

Since the dipolar field depends on the amplitude of oscillations and the distance, and due to the fact that this field affects the coupling strength between the oscillators, then, the phase locking bandwidth and the strength of interaction may vary according to the external magnetic field and the separation between the STNOs.

For two oscillators coupled through dipolar interaction, the polarity of the applied voltage may increase the phase locking bandwidth. This is because, when the two STNOs have similar voltages in magnitude but with opposite polarity their magnetizations may be oriented anti-parallel which is a configuration that minimizes energy and thus favors coupling.

The dipolar interaction can be strong enough to excite oscillations on a STNO that would be static if isolated. Hence, one could cause oscillations on a group of STNOs without applying a current to each one of them. This will be considered for the PhD.

There are some phenomena that still have to be understood in a deeper way, like the numerical-analytical disagreement of the V_{stat} voltage, some features in the diagram of the asymmetric device and the absence of coupling when injection locking was studied for some specific cases.

For future work during the PhD, the synchronization between more than two oscillators will be considered with different geometrical arrangements. Besides, injection locking can be studied with a RF signal applied though the magnetic field instead of the current. Additionally, other simulations considering higher temperatures may be performed, because this parameter affects the extension of the TS zone in the diagram of the single STNO.

8. References

[1] O'Handley, R., 2000. *Modern Magnetic Materials*. New York: Wiley, pp.145-147.

[2] M. Julliere, “Tunneling between ferromagnetic films,” *Phys. Lett. A* 54, 225 (1975).

[3] W. F. Brown, “Thermal fluctuations of a single-domain particle,” *Phys. Rev.* **130**, pp. 1677–1986 (1963); doi: 10.1103/PhysRev.130.1677.

[4] J. C. Maxwell, *A Treatise on Electricity and Magnetism*, vol. 2, §437 and §438, Clarendon Press,

Oxford, 1881.

[5] B. O. Peirce, *Elements of the Theory of the Newtonian Potential Function*, Ginn & Company, Boston, 1902, §69.

[6] C. L. B. Shuddemagen, “The demagnetizing factors for cylindrical iron rods,” *Proc. Am. Acad. Arts Sci.* **43**, pp. 185–256 (1907).

[7] J. C. Slonczewski, “Current-driven excitation of magnetic multilayers,” *J. Magn. Magn. Mater.* **159**, pp. L1–L7 (1996); doi: 10.1016/0304-8853(96)00062-5.

[8] T. L. Gilbert and J. M. Kelly,“Anomalous rotational damping in ferromagnetic sheets,” in *Conference on Magnetism and Magnetic Materials*, Pittsburgh, PA, June 14–16, 1955, American Institute of Electrical Engineers, New York, October 1955, pp. 253–263.

[9] T. L. Gilbert, “A phenomenological theory of damping in ferromagnetic materials,” *IEEE Trans. Magn.* **40**, pp. 3443–3449 (2004); doi: 10.1109/TMAG.2004.836740.

[10] Ebels, U., Houssameddine, D., Firastrau, I., Gusakova, D., Thirion, C., Dieny, B. and Buda-Prejbeanu, L., 2008. Macrospin description of the perpendicular polarizer-planar free-layer spin-torque oscillator. *Physical Review B*, 78(2).

[11] Slavin, A. and Tiberkevich, V., 2009. Nonlinear Auto-Oscillator Theory of Microwave Generation by Spin-Polarized Current. *IEEE Transactions on Magnetics*, 45(4), pp.1875-1918.

[12] Pikovsky, A., Rosenblum, M. and Kurths, J., 2001. *Synchronization*. Cambridge: Cambridge University Press, pp.7-53.